Published Online: 14 March, 2016 | Supp Info: http://doi.org/10.1083/jcb.201509085

Collagen-derived matricryptins promote inhibitory nerve terminal formation in the developing neocortex

Jianmin Su,[1] Jiang Chen,[1] Kumiko Lippold,[1] Aboozar Monavarfeshani,[1,2] Gabriela Lizana Carrillo,[1] Rachel Jenkins,[3] and Michael A. Fox[1,2]

[1]Virginia Tech Carilion Research Institute, Roanoke, VA 24016
[2]Department of Biological Sciences and [3]Department of Biochemistry, Virginia Polytechnic Institute and State University, Blacksburg, VA 24061

Inhibitory synapses comprise only ∼20% of the total synapses in the mammalian brain but play essential roles in controlling neuronal activity. In fact, perturbing inhibitory synapses is associated with complex brain disorders, such as schizophrenia and epilepsy. Although many types of inhibitory synapses exist, these disorders have been strongly linked to defects in inhibitory synapses formed by Parvalbumin-expressing interneurons. Here, we discovered a novel role for an unconventional collagen—collagen XIX—in the formation of Parvalbumin$^+$ inhibitory synapses. Loss of this collagen results not only in decreased inhibitory synapse number, but also in the acquisition of schizophrenia-related behaviors. Mechanistically, these studies reveal that a proteolytically released fragment of this collagen, termed a matricryptin, promotes the assembly of inhibitory nerve terminals through integrin receptors. Collectively, these studies not only identify roles for collagen-derived matricryptins in cortical circuit formation, but they also reveal a novel paracrine mechanism that regulates the assembly of these synapses.

Introduction

Schizophrenia is a complex brain disorder characterized by alterations in cognitive function (including impairment in attention, sensorimotor gating, and memory), acquisition and expression of behaviors not seen in healthy individuals (including hallucination and obsession), and loss of behaviors normally present in healthy individuals (including apathy, neglect, and social withdrawal). Mounting evidence suggests that schizophrenia-associated behaviors result from alterations in the assembly and function of synapses, specialized connections between neurons that facilitate information transfer within neural circuits (Gonzalez-Burgos et al., 2010, 2011; Lewis et al., 2012; Yin et al., 2012). Synapses are broadly categorized into at least two types: synapses whose activity increases the probability of activity in postsynaptic partner neurons are excitatory, and synapses that reduce the probability of activity in partner neurons are inhibitory. Inhibitory synapses comprise only ∼20% of total synapses but play essential roles in controlling neural activity. In fact, perturbing inhibitory synapse assembly or function has been associated with schizophrenia, as well as other debilitating neurological conditions such as autism and epilepsy (Rubenstein and Merzenich, 2003; Gonzalez-Burgos et al., 2010, 2011; Sgadò et al., 2011; Lewis et al., 2012; Yin et al., 2012; Hunt et al., 2013). Although many types of inhibitory synapses exist, schizophrenia and related neurodevelopmental disorders have been linked to defects in inhibitory synapses formed by Parvalbumin (Parv)-expressing interneurons (Benes and Berretta, 2001; Schwaller et al., 2004; Belforte et al., 2010; Gonzalez-Burgos et al., 2010, 2011; Sgadò et al., 2011; Gonzalez-Burgos and Lewis, 2012; Lewis et al., 2012; Wöhr et al., 2015). Unfortunately, despite their clear importance, we lack a full understanding of the molecular mechanisms responsible for the assembly of Parv$^+$ synapses.

With the goal of identifying molecular mechanisms underlying Parv$^+$ synapse formation, our attention was drawn to collagen XIX, a nonfibrillar collagen associated with familial schizophrenia (Liao et al., 2012) and expressed by neurons in the mammalian brain (Sumiyoshi et al., 1997; Su et al., 2010). Here we set out to answer whether the loss of collagen XIX resulted in schizophrenia-related behaviors using a targeted mouse mutant that lacks this collagen (Sumiyoshi et al., 2004). Our data reveal that collagen XIX–deficient mutants exhibit several schizophrenia-related traits in addition to spontaneous seizures and an increased susceptibility to drug-induced seizures. Moreover, the absence of collagen XIX disrupts the formation of Parv$^+$ inhibitory axosomatic synapses in cerebral cortex (CTX).

Like many nonfibrillar collagens, collagen XIX harbors a C-terminal domain that can be proteolytically shed as a matricryptin,

Correspondence to Michael A. Fox: mafox1@vtc.vt.edu

Abbreviations used in this paper: CTX, cerebral cortex; DIV, day in vitro; EEG, electroencephalograph; EMG, electromyograph; GABA, γ-aminobutyric acid; GAD, glutamate decarboxylase; IHC, immunohistochemistry; ISH, in situ hybridization; KO, knockout; lumVGAT, luminal domain of vesicular GABA transporter; NC, noncollagenous; P, postnatal day; pp, prepulse; PPI, prepulse inhibition; PTZ, pentylenetetrazol; qPCR, quantitative real-time PCR; VGluT, vesicular glutamate transporter; WT, wild type.

a bioactive molecule that exhibits functions distinct from those of the full-length matrix molecule from which it was released (Ramont et al., 2007). Outside of the nervous system, matricryptins influence many aspects of cell behavior (Kalluri, 2003). In the nervous system, matricryptins contribute to axon outgrowth, synaptogenesis, and synaptic plasticity in worms, flies, fish, and mice (Ackley et al., 2001; Fox et al., 2007; Meyer and Moussian, 2009; Su et al., 2012; Wang et al., 2014). Here we tested whether the same was true for matricryptins from collagen XIX. We discovered that the C-terminal peptide from collagen XIX is sufficient to trigger the formation of inhibitory nerve terminals by signaling through integrin receptors. Collectively, these results identify novel roles for collagen XIX in the formation of inhibitory synapses and provide insight into why the loss of this collagen leads to phenotypes associated with complex brain disorders.

Results

Loss of collagen XIX leads to schizophrenia-related behaviors and seizures

A recent study identified a microdeletion of ∼4.4 Mb at chromosome 6q12-13 in a cohort of patients with familial schizophrenia (Liao et al., 2012). This region contains the coding sequence of collagen XIX, as well as a small number of other genes. To test whether the deletion of collagen XIX results in schizophrenia-related behaviors, we assessed the performance of mutants lacking collagen XIX (*col19a1*$^{-/-}$) in a battery of behavioral assays. First, we assessed sensorimotor gating by testing prepulse inhibition (PPI) of the acoustic startle response (Fig. 1 A). In wild-type (WT) mice, the acoustic startle is inhibited if it is preceded by low decibel sounds (Fig. 1 B). Mice lacking collagen XIX display significant impairment in this response (Fig. 1 B) but do not display defects in basal startle responses (Fig. 1 C). Second, to test whether the absence of collagen XIX leads to negative symptoms associated with schizophrenia (such as apathy, self-neglect, and social withdrawal), we assessed nesting behaviors (Belforte et al., 2010; Albrecht and Stork, 2012; Pedersen et al., 2014). Singly housed mice were given a cotton nestlet, and their ability to build a nest overnight was assessed (Fig. 1 D; Deacon, 2006). Although WT mice consistently generated structured nests, *col19a1*$^{-/-}$ mutants failed to generate nests (Fig. 1, E and F). Third, to assess social affiliation and memory, we assessed behavior with the Crawley sociability and preference for social novelty protocol (Fig. 1, G–J; Moy et al., 2004). Although *col19a1*$^{-/-}$ mutants exhibited normal preference for novel conspecifics (versus an empty chamber; Fig. 1 H), they spent equal time investigating familiar and novel conspecifics, revealing a deficit in social memory (Fig. 1 J). Finally, we tested exploration in open-field assays (Fig. 1, K–M). Overall exploration of *col19a1*$^{-/-}$ mutants was significantly reduced compared with littermate controls (Fig. 1 L).

To confirm that defects in PPI, nest building, open-field exploration, and social memory assays did not result from general motor defects in mutants, we used rotarod and wheel-running assays (Fig. 1, N–R). No significant differences were observed in mutants and littermate controls in these assays, suggesting that the behavioral defects described were not the result of general motor defects in *col19a1*$^{-/-}$ mutants.

Interestingly, while breeding mice for these behavioral assays, we observed *col19a1*$^{-/-}$ mutants exhibiting spontaneous motor seizures and absence-like seizures. These phenotypes are associated with inhibitory circuit dysfunction, and schizophrenia is 6–12 times more common in patients with seizures than in healthy controls (Sachdev, 1998). To document seizures in these mutants, we performed electroencephalograph (EEG) and electromyograph (EMG) recordings (Fig. 2 A). Although few, if any, seizures were observed in WT mice, we observed abnormal spike-wave activity and rapid spiking waves in all *col19a1*$^{-/-}$ mutants analyzed (n = 9; Fig. 2 B), with some seizures persisting for 10 min (Fig. 2 C). We observed a mean of ∼40 seizures in *col19a1*$^{-/-}$ mutants over 5 d (37.7 ± 5.4 [mean ± SEM] seizure-like events, n = 9, versus 5.8 ± 4.8 in controls, n = 6). Although this number seems high, it is comparable to other mouse models of schizophrenia (e.g., 51.5 ± 2.5 seizure events in *reln*$^{rl/+}$ heterozygotes, n = 2; Iafrati et al., 2014).

In addition to measuring spontaneous seizures, we assessed *col19a1*$^{-/-}$ mutant responses to seizure-inducing drugs. In control mice, low doses of pentylenetetrazol (PTZ), a γ-aminobutyric acid (GABA) antagonist, induced mild motor seizures (Fig. 2, D and E). In *col19a1*$^{-/-}$ mutants, similar doses of PTZ resulted in severe seizures (Fig. 2, D and E) that in many cases were lethal (n = 12 of 14; Fig. 2 D). Collectively, these results demonstrate that *col19a1*$^{-/-}$ mutants exhibit schizophrenia-related behaviors and are more susceptible to seizures—two phenotypes linked to inhibitory circuits (Takahashi et al., 2012; Krook-Magnuson et al., 2013; Rossignol et al., 2013).

Collagen XIX is expressed by cortical interneurons and is necessary for inhibitory synapse formation

Collagen XIX is a lesser-studied collagen, with just a handful of articles about its role in mammals, especially in regard to nervous system development and function. To elucidate how collagen XIX loss leads to altered behavior and seizures, we used EvoCor, a novel bioinformatics platform that predicts putative functional linkage between genes based on their phylogenetic profile and expression patterns (Dittmar et al., 2014). When we used this platform to analyze *col19a1*, the gene encoding collagen XIX, we were surprised to discover that the majority of top candidates were genes enriched in the brain and linked to synaptic development or function (Fig. 3, A–C). In fact, more than half of the candidate related genes appeared enriched in mouse CTX according to the Allen Brain Atlas (Lein et al., 2007). It is important to point out that analysis of other collagens with this approach, even those implicated in synaptogenesis, did not result in candidate lists containing genes enriched in CTX or implicated in synaptic biology (Fig. S1).

The unexpected results from EvoCor analysis led us to ask two questions: Is collagen XIX expressed in CTX? and, Is collagen XIX involved in the formation of synapses in mouse CTX? To answer the first question, we performed in situ hybridization (ISH; Fig. 3 D). As expected from EvoCor analysis, *col19a1* mRNA was enriched in CTX compared with other brain regions (Fig. 3, D–F). Not all cells in CTX expressed *col19a1* mRNA; rather, its expression was restricted to a small subset of neurons (Fig. 3, H–J). Furthermore, *col19a1*-expressing cells contained glutamate decarboxylase (GAD67 or GAD65), enzymes required for converting glutamate into GABA in inhibitory CTX interneurons (Fig. 3 K), although not all GAD-expressing cells generated *col19a1* mRNA.

Many types of inhibitory interneurons are present in the mammalian CTX. We next sought to understand which classes of interneurons expressed this collagen. By coupling ISH with

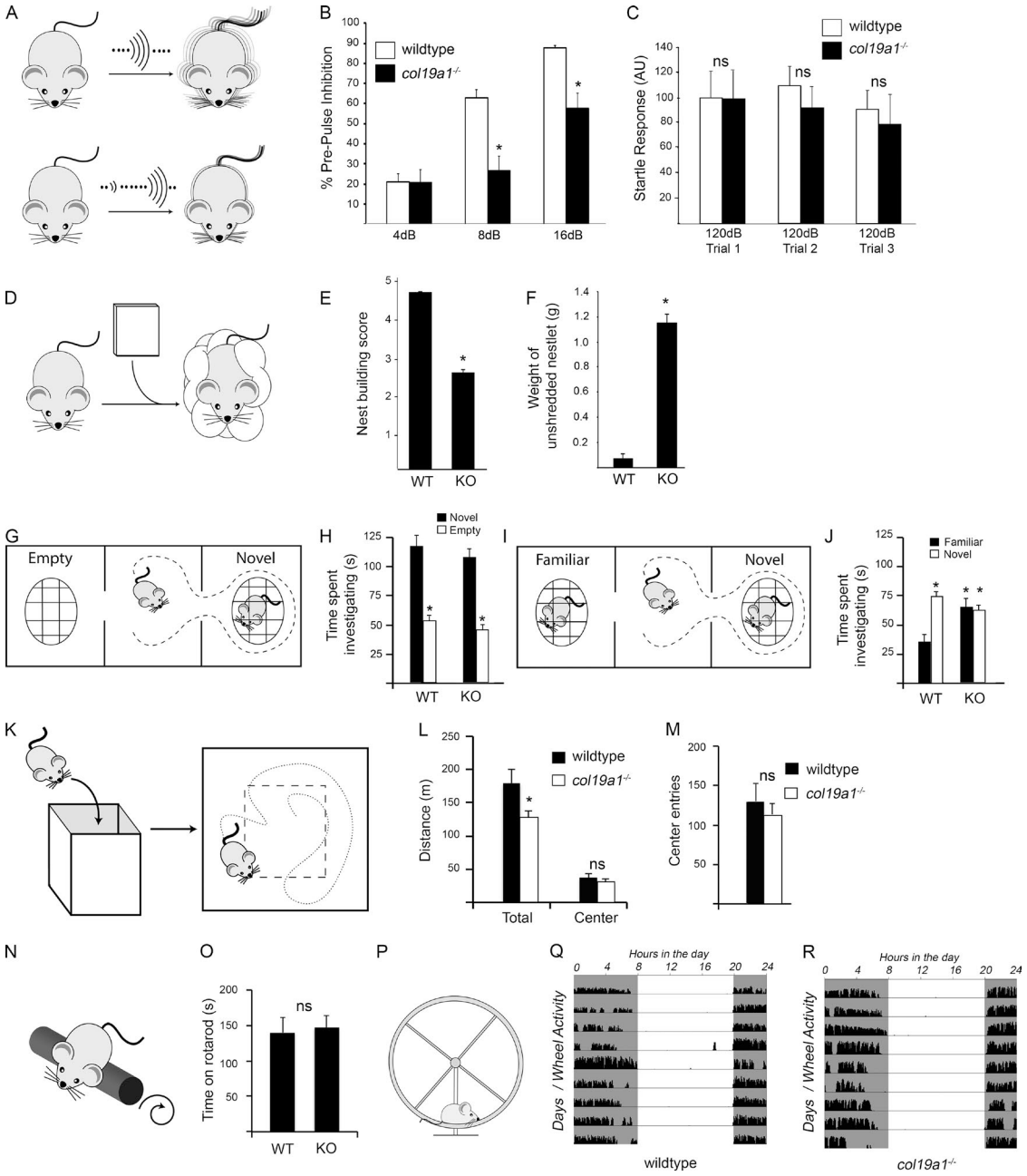

Figure 1. **Mice lacking collagen XIX display schizophrenia-related behaviors.** (A) Schematic illustration of PPI of the acoustic startle response. (B) *Col19a1*$^{-/-}$ mutant mice (knockout [KO]) display impairment in PPI. Data are mean ± SEM. *, Differs from WT by P < 0.01, Tukey–Kramer test for difference between means; *n* = 27 WT and 39 KO. Prepulse intensities (4, 8, and 16 dB) indicate the intensity above background noise (65 dB). (C) No significant differences were observed in basal acoustic startle of WT or KO to a 120-dB noise. Data are mean ± SEM. ns, no statistical difference by Tukey–Kramer test. AU, arbitrary units. (D) Schematic illustration of nest-building behavior assay. (E and F) *Col19a1*$^{-/-}$ mutant mice displayed reduced nest-building behaviors. Nests were scored manually by their appearance after 12 h (E) or weighing unused nestlets after 12 h (F). Data are mean ± SEM. *, Differs from WT by P < 0.01 by Tukey–Kramer test for difference between means; *n* = 21 WT and 25 KO. (G and I) Schematic illustration of sociability (G) and social memory assays (I). (H) *Col19a1*$^{-/-}$ mutant mice displayed normal preference for novel conspecifics versus empty chambers. Data are mean ± SEM. *, Differs from interaction with conspecific by P < 0.01 by Tukey–Kramer test for difference between means; *n* = 15 WT and 25 KO. (J) *Col19a1*$^{-/-}$ mutant mice displayed abnormal indifference to novel and familiar conspecifics. Data are mean ± SEM. *, Differs from interaction with familiar conspecific by P < 0.01 by Tukey–Kramer test for difference between means; *n* = 15 WT and 25 KO. (K) Schematic illustration of open-field assay. (L and M) *Col19a1*$^{-/-}$ mutant mice displayed reduced exploration in open-field assays. Data are mean ± SEM. *, Differs from WT by P < 0.01. ns, P > 0.05 by Tukey–Kramer test for difference between means; *n* = 29 WT and 42 KO. (N) Schematic illustration of rotarod assay. (O) *Col19a1*$^{-/-}$ mutant mice performed as well as controls in an accelerating rotarod assay. Data are mean ± SEM. ns, no significant difference by Student's *t* test; *n* = 21 WT and 25 KO. (P) Schematic illustration of wheel-running assay. (Q and R) Actograms show that *col19a1*$^{-/-}$ mutant mice display normal levels of activity and photoentrainment. Each row of data indicates the wheel activity for a 24-h period. Gray regions indicate periods of wheel-running activity in darkness.

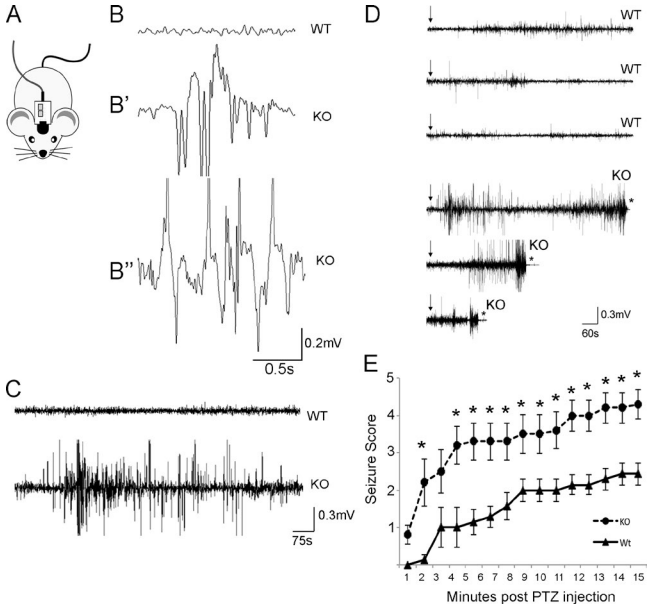

Figure 2. **Mice lacking collagen XIX exhibit spontaneous seizures and are more susceptible to drug-induced seizures.** (A) Schematic illustration of the EEG/EMG headmounts. (B) EEG traces from WT (B) and *col19a1*$^{-/-}$ mutant mice (KO; B′ and B″). B′ shows a recording obtained during an absence-like seizure in a KO. B″ shows a recording obtained during a myoclonic seizure in a KO. (C) EMG traces from WT and KO. (D) EMG traces showing 15 min of activity in three WT and three KO after the delivery of PTZ (indicated by the arrows). Asterisks indicate death. (E) Manual seizures scores for WT and KO mice were recorded for 15 min after the delivery of PTZ. Data are mean ± SEM. *, Differs from controls by $P < 0.05$ by Tukey–Kramer test for difference between means; $n = 7$ WT and 10 KO.

immunohistochemistry (IHC), we discovered that *col19a1* mRNA was present in subsets of Calbindin- and Somatostatin-expressing interneurons, but not in Calretinin-expressing interneurons (Fig. 3, L–N). Finally, we asked whether Parv-expressing interneurons generated collagen XIX. This question seemed particularly pertinent because this class of interneurons has been implicated in schizophrenia and seizures. We used two approaches to address this question: double ISH with riboprobes against both *col19a1* and *parv* (the gene encoding Parv) and *col19a1* ISH in *parv-cre::thy1-stop-yfp* transgenic mice. We detected no *col19a1*$^{+}$/*parv*$^{+}$ neurons with double ISH at postnatal day 14 (P14), and less than 3% of *col19a1*-expressing cells contained *parv* mRNA in adult CTX (2.8% ± 0.8% [mean ± SD] of *col19a1*$^{+}$ neurons contained *parv* mRNA at P56; $n = 3$; Fig. 3, O and P). Likewise, only a small fraction of *col19a1*$^{+}$/YFP^{+} neurons in P56 *parv-cre::thy1-stop-yfp* transgenic tissues (8.1% ± 1.2% of *col19a1*$^{+}$ neurons; $n = 3$; Fig. 3 Q) contained YFP at P56. These results demonstrate that most *col19a1*-expressing neurons do not generate Parv, and vice versa.

Having determined that *col19a1* mRNA was generated by subsets of interneurons, we next addressed whether it was necessary for cortical synaptogenesis. Our first hint that it may be involved in this process came from expression analysis that showed the peak of *col19a1* mRNA expression coinciding with the peak of synaptogenesis (Fig. 3 G). To test whether synaptogenesis was impaired in *col19a1*$^{-/-}$, we performed a broad IHC screen with antibodies that label different types of nerve terminals. First, we investigated the distribution of several markers of excitatory nerve terminals (i.e., vesicular glutamate transporter 1 [VGluT1] and VGluT2) in *col19a1*$^{-/-}$ mutants and littermate controls. No obvious differences were observed in the distribution, density, or morphology of excitatory nerve terminals in the developing visual cortex (vCTX) or prefrontal cortex (pfCTX) in mutants (Figs. 4, A, C, E, F, J, K, O, and Q; and Fig. S2, A–J). Likewise, we detected no difference in the number of dendritic spines on cortical layer V pyramidal neurons in *col19a1*$^{-/-}$ mutants (Fig. S2, K–M).

We next assessed the distribution of inhibitory nerve terminals in mutant and control CTX with antibodies against GAD67 and Synaptotagmin 2 (Syt2), a vesicle-associated calcium sensor present in inhibitory terminals in CTX (Sommeijer and Levelt, 2012; Fig. 5 A and Fig. S3, A–F). Significantly fewer Syt2^{+} nerve terminals were observed in layers II/III and V of the developing vCTX and pfCTX in mutants (Figs. 4, A–D, G, H, L, and M; and Fig. S2, A–J). Likewise, we detected a significant reduction in GAD67^{+} nerve terminals in the cortex of *col19a1*$^{-/-}$ mutants (Fig. S2, N–P). Supporting these data, levels of Syt2, GAD isoforms (GAD67 and GAD65), and Gephyrin (Geph; a postsynaptic scaffolding protein at inhibitory synapses) were significantly reduced in protein extracts or synaptosome fractions of mutant CTX (Fig. 4, O–R). Importantly, differences in Syt2^{+} inhibitory nerve terminal distribution did not reflect a delay in development, because significant reductions persisted into adulthood in mutants (Figs. 4, I and N; and Fig. S2, Q–S). Nor did we detect alterations in the number or distribution of Syt2- or Parv-expressing inhibitory interneurons in the absence of collagen XIX (Fig. S4, A–F). Together, these studies reveal a novel role for collagen XIX in the formation of inhibitory nerve terminals in mouse CTX.

In looking at the distribution of Syt2^{+} nerve terminals in mutant CTX, especially in adult tissues (Fig. S2, Q–S), it became clear that fewer axosomatic synapses were present in the absence of collagen XIX. One class of axosomatic synapses are generated by Parv^{+} GABAergic interneurons; therefore, to test whether Syt2^{+} terminals originated from Parv^{+} GABAergic interneurons, we performed Syt2-IHC in cortical sections from *parv-cre::thy1-stop-yfp* transgenic mice. More than 95% of Syt2^{+} terminals in vCTX and pfCTX contained YFP in these tissues, indicating they originated from Parv^{+} interneurons (Fig. S3 G; Sommeijer and Levelt, 2012).

Parv^{+} interneurons are known to generate axosomatic synapses onto two main types of neurons in mouse CTX: excitatory pyramidal neurons and other Parv^{+} interneurons (Pi et al., 2013; Pfeffer et al., 2013). We therefore crossed *col19a1*$^{-/-}$ mutants with *thy1-yfp (line H)* mice (which selectively label layer V pyramidal neurons in cortex; Feng et al., 2000) and *parv-cre::thy1-stop-yfp* mice (which label Parv^{+} GABAergic interneurons) to assess axosomatic terminals in the absence of collagen XIX. Significantly fewer Syt2^{+} axosomatic nerve terminals were observed on both cell types in CTX of mutants (Fig. 5, B–G). To test whether this result reflected a loss of inhibitory nerve terminals or the loss of synapses, we immunostained for both pre- and postsynaptic markers (i.e., Syt2 and Geph) in pfCTX in mutants and controls crossed to *thy1-yfp (line H)* and *parv-cre::thy1-stop-yfp* reporter mice (Fig. 5, H and I). We observed not only a reduction in Syt2^{+} nerve terminals, but also a statistically significant reduction in Geph^{+} postsynaptic elements, suggesting that few inhibitory axosomatic synapses were present in the absence of collagen XIX (Fig. 5, J and K). Because Parv^{+} synapses have been strongly linked to schizophrenia and seizures, these results provide a mechanism for how collagen XIX loss may lead to behavioral abnormalities.

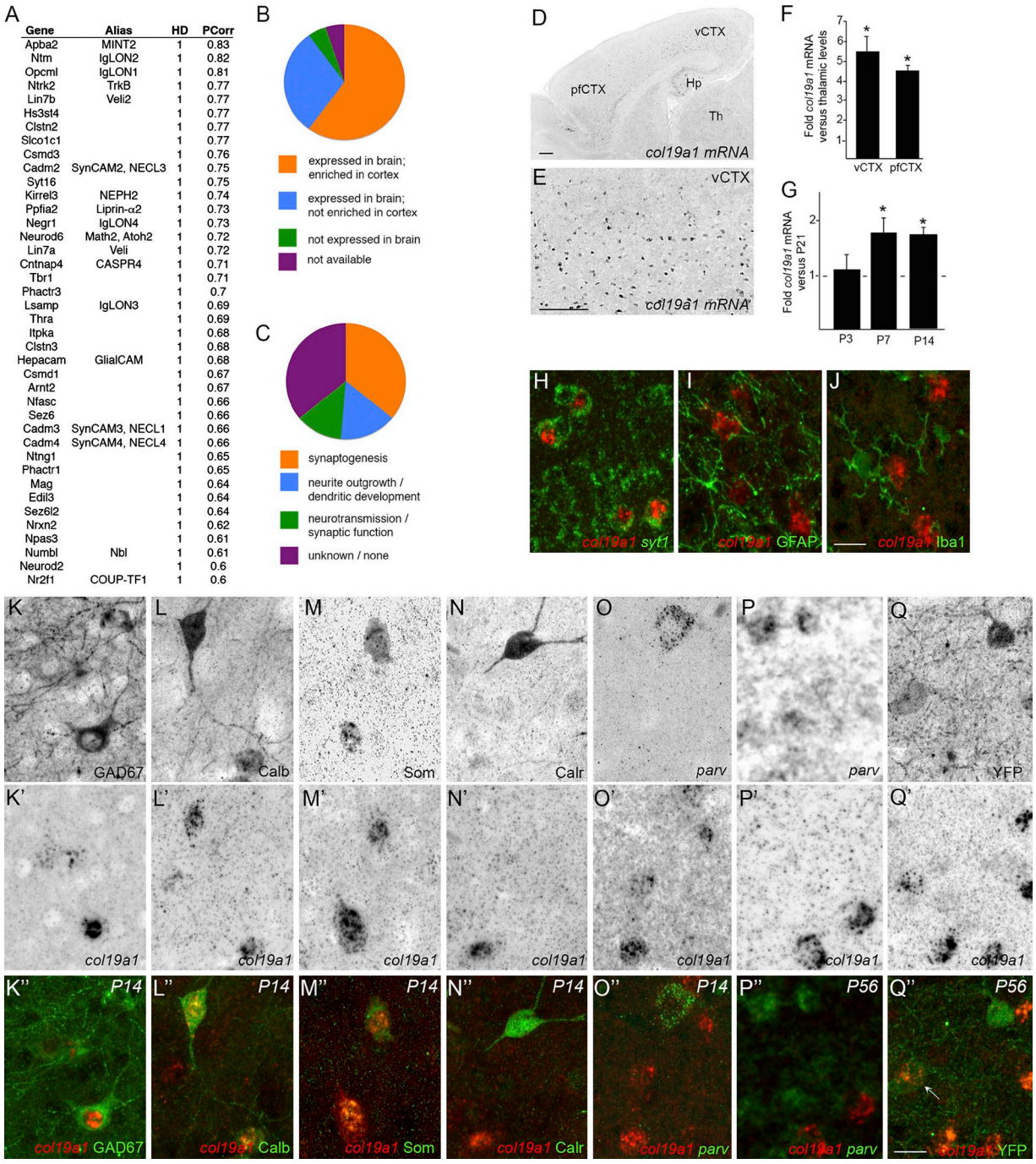

Figure 3. **Collagen XIX is expressed by subsets of cortical interneurons.** (A) Top genes predicted by EvoCor analysis as being functionally related to mouse *col19a1* based on evolutionary history and tissue-wide gene expression patterns. HD, Hamming distance; PCorr, Pearson correlation. (B) Tissue distribution of 40 genes listed in A. (C) >60% of top genes predicted by EvoCor analysis are implicated in contributing to synapse formation or function. (D and E) ISH for *col19a1* mRNA in P8 mouse brain. (E) High-magnification image of *col19a1* mRNA distribution in visual cortex. Th, dorsal thalamus. Bars, 200 μm. (F) qPCR shows relative levels of *col19a1* mRNA expression in vCTX and pfCTX versus dorsal thalamus. Expression levels normalized to *gapdh*. Data are mean ± SEM; $n = 4$. *, Differs from thalamic expression by $P < 0.0001$ by one-way analysis of variance. (G) qPCR shows that *col19a1* mRNA expression is developmentally regulated. Expression levels normalized to *gapdh*. Data are mean ± SEM; $n = 3$. *, Differs from expression at P21 by $P < 0.0001$ by one-way analysis of variance. (H–J) ISH reveals that *col19a1* is generated by *syt1*-expressing neurons (H) but not by astrocytes (I) or microglia (J) in P14 mouse cortex. H shows a double ISH experiment, whereas I and J represent ISH-IHC experiments. Bar, 25 μm. (K–N) ISH reveals that *col19a1* is generated by GAD67$^+$, Calb$^+$, and Som$^+$ interneurons (K–M) but not Calr$^+$ interneurons (N), as determined by ISH-IHC. (O–Q) Most *col19a1*-expressing neurons do not generate Parv. Double ISH (O and P) and ISH-IHC (with *parv-cre::thy1-stop-yfp* tissue; Q) revealed that only a small fraction (if any) of *col19a1*-expressing neurons generate Parv. Ages of each experiment are indicated in K″–Q″. Bar, 25 μm.

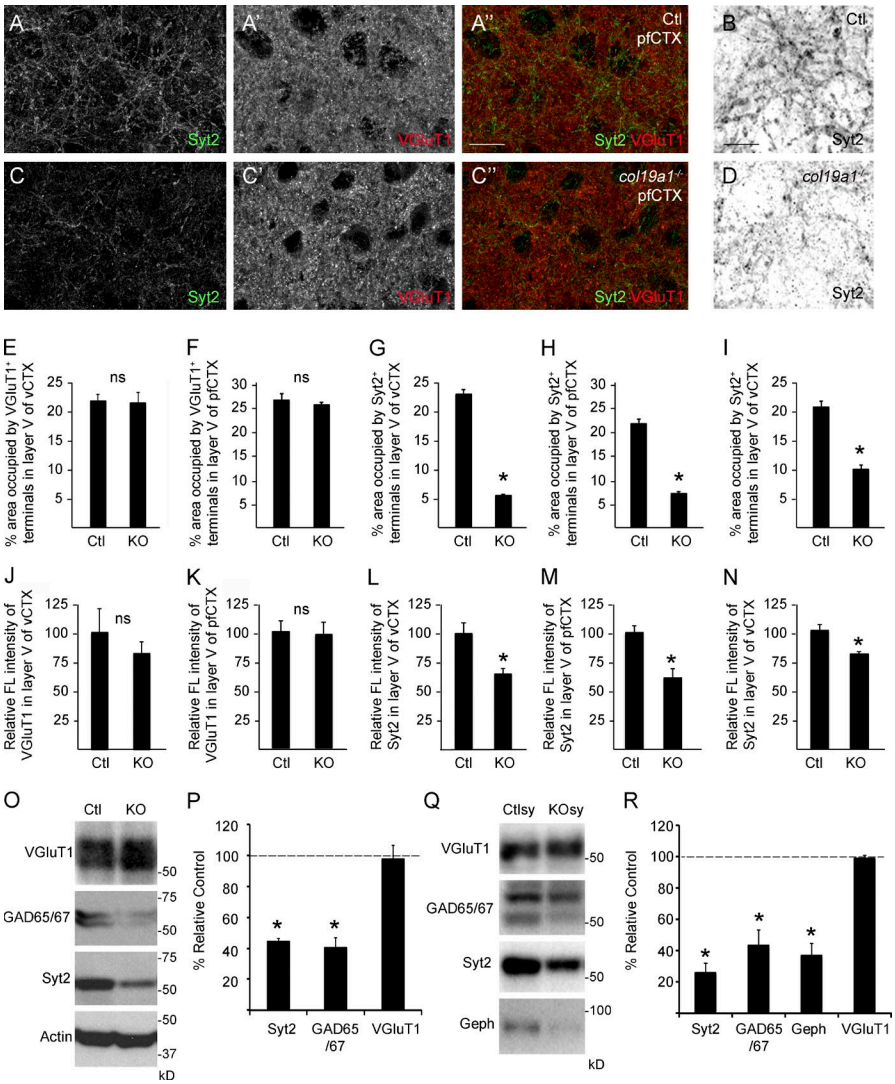

Figure 4. **Loss of collagen XIX leads to impaired inhibitory synapse formation in mouse CTX.** (A–D) Immunostaining for Syt2 and VGluT1 in layer V of pfCTX in P11 WT controls (Ctl) and *col19a1*$^{-/-}$ mutants (KO). (B and D) High-magnification images of Syt2-immunostaining from layer V of pfCTX in P11 WT controls (Ctl) and *col19a1*$^{-/-}$ mutants. A–D depict Syt2-immunolabeling; A′ and C′ depict VGluT1-immunolabeling; A″ and C″ depict merged overlay of Syt2 and VGluT1 immunolabeling. Bars: (A″) 25 µm; (B) 5 µm. (E–H) Area occupied by VGluT1 and Syt2 immunoreactivity (IR) in layer V of pfCTX and vCTX in P11 control and KO. Data are mean ± SEM; $n = 4$. *, Differs from control by $P < 0.001$ by Student's *t* test. ns, no statistical difference by Student's *t* test. (I) Area occupied by Syt2 IR in layer V of vCTX in P56 control and KO. Data are mean ± SEM; $n = 4$. *, Differs from controls by $P < 0.001$ by Student's *t* test. (J–M) Mean fluorescence intensity of VGluT1 and Syt2 IR in layer V of pfCTX and vCTX in P11 control and KO. Data are mean ± SEM; $n = 4$. *, Differs from control by $P < 0.001$ by Student's *t* test. ns, no statistical difference by Student's *t* test. (N) Mean fluorescence intensity of Syt2 IR in layer V of vCTX in P56 control and KO. Data are mean ± SEM; $n = 4$. *, Differs from control by $P < 0.001$ by Student's *t* test. (O–R) Western blots show reduced levels of GAD65/67 and Syt2 (but not VGluT1) in protein extracts (O and P) and synaptosome fractions (sy; Q and R) from KO CTX versus control (dashed line). Data are mean ± SEM; $n = 4$. *, Differs from control by $P < 0.001$ by Student's *t* test.

A C-terminal fragment of collagen XIX is sufficient to induce inhibitory nerve terminal formation

To understand how collagen XIX influences synaptogenesis, we generated dissociated neuronal cultures from CTX or hippocampus (HP). These cultures contained interneurons capable of generating Syt2$^+$ nerve terminals (Fig. 6, A and B). Moreover, these cultures mimicked our in vivo results in two ways: (1) Syt2$^+$ terminals formed inhibitory axosomatic terminals (Fig. 6, A and B), and (2) Syt2$^+$ terminals failed to form in cultures generated from *col19a1*$^{-/-}$ mutant mice (Fig. 6 C).

Collagen XIX is a nonfibrillar collagen with five collagenous domains, each flanked by noncollagenous (NC) domains (Fig. 6 D). Recent research indicates that the C-terminal NC domain (i.e., NC1) is cleaved off by Plasmin and functions as a matricryptin (Oudart et al., 2015). Importantly, Plasmin is expressed in mouse vCTX and pfCTX (Oray et al., 2004; Castorina et al., 2013). Therefore, based on roles of other synaptogenic matricryptins, we hypothesized that the NC1 domain of collagen XIX might trigger inhibitory nerve terminal formation. To test this, we synthesized mouse NC1 (mNC1) and applied it to WT neurons (Fig. 6, E–H). After 2 d, we observed a three- to fourfold increase in Syt2$^+$ puncta in the presence of mNC1 (Fig. 6, E–H) or human NC1 (hNC1; Fig. 6 G). Application of mNC1 peptides also increased GAD67$^+$ puncta in these assays (Fig. S5, A–C). Other NC domains of collagen XIX (e.g., NC2, NC3, and NC6) failed to trigger inhibitory nerve terminal formation in these assays (Fig. 6, G and H; and not depicted). Importantly, NC1-stimulated Syt2$^+$ puncta appeared to be functionally active, because (a) they could be labeled by the live application of antibodies against the luminal domain of vesicular GABA transporter (lumVGAT; Fig. 6 I; Martens et al., 2008), and (b) they colocalized with Geph (Fig. 6 J).

These results suggest that the NC1 domain of collagen XIX promotes the assembly of inhibitory nerve terminals. Next, we tested whether NC1 peptides were sufficient to rescue synaptic defects in neurons from *col19a1*$^{-/-}$ mutants. Indeed, mNC1 peptides rescued the loss of Syt2$^+$ puncta in *col19a1*$^{-/-}$ neurons (Fig. 6, K–M). Thus, the NC1 domain of collagen XIX is sufficient to trigger inhibitory nerve terminal formation.

Mechanisms underlying the synaptogenic function of the NC1 domain of collagen XIX

To determine how the NC1 domain of collagen XIX triggers nerve terminal assembly, we first sought to answer whether it acted as a synaptic primer (like growth factors, morphogens, or neurotrophic factors) or whether it directly induced the assembly of presynaptic machinery into a nerve terminal (like

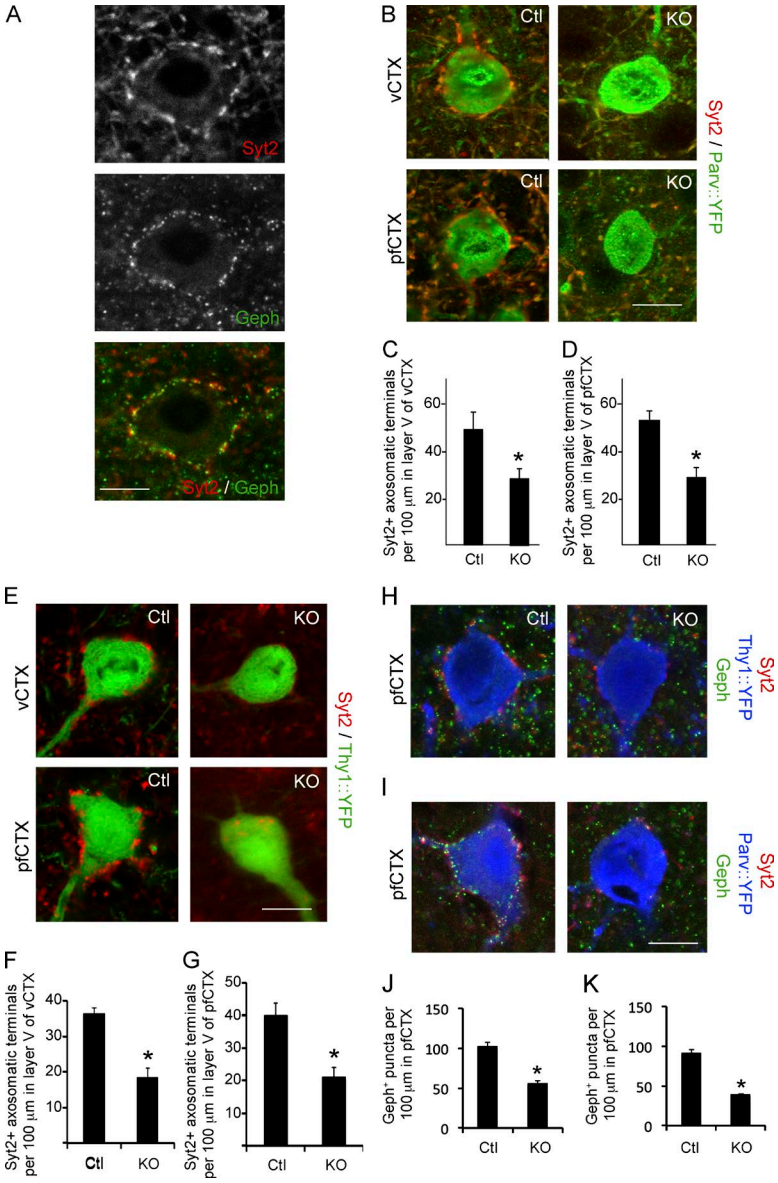

Figure 5. **Loss of collagen XIX leads to reduced numbers of axosomatic inhibitory synapses in mouse CTX.** (A) Syt2+ axosomatic nerve terminals colocalize with Geph in pfCTX. Bar, 8 µm. (B) Syt2+/YFP+ axosomatic synapses were analyzed in single optical sections of *col19a1*$^{+/+}$*::parv-cre::thy1-stop-yfp* (Ctl) and *col19a1*$^{-/-}$*::parv-cre::thy1-stop-yfp* (KO) mice. Bar, 12 µm. (C and D) Reduced numbers of Syt2+ axosomatic synapses (per unit length of cell soma) were detected in *col19a1*$^{-/-}$*::parv-cre::thy1-stop-yfp* (KO) vCTX and pfCTX compared with controls. Data are mean ± SEM; *n* = 3. *, Differs from control by P < 0.001 by Student's *t* test. (E) Syt2+ axosomatic synapses were analyzed in single optical sections of *col19a1*$^{+/+}$*::thy1-yfp lineH* (Ctl) and *col19a1*$^{-/-}$*::thy1-yfp lineH* (KO) mice. Bar, 12 µm. (F and G) Reduced numbers of Syt2+ axosomatic synapses (per unit length of cell soma) were detected on YFP+ excitatory neurons in *col19a1*$^{-/-}$*::thy1-yfp lineH* vCTX and pfCTX compared with control. Data are mean ± SEM; *n* = 3. *, Differs from control by P < 0.001 by Student's *t* test. (H) IHC for Geph and Syt2 in layer V of pfCTX in P21 *col19a1*$^{+/+}$*::thy1-yfp (line H)* (Ctl) and *col19a1*$^{-/-}$*::thy1-yfp (line H)* mutants (KO). Layer V pyramidal cells are labeled in *thy1-yfp (line H)* mice. Confocal images are single optical sections. (I) IHC for Geph and Syt2 in layer V of pfCTX in P21 *col19a1*$^{+/+}$*::parv-cre::thy1-stop-yfp* (Ctl) and *col19a1*$^{-/-}$*::parv-cre::thy1-stop-yfp* mutants (KO). Parv+ interneurons are labeled in *parv-cre::thy1-stop-yfp* mice. Confocal images are single optical sections. (J) Reduced numbers of Geph+ postsynapses (per unit length of cell soma) were detected in *col19a1*$^{-/-}$*::thy1-yfp (line H)* mutant (KO) pfCTX compared with levels in control. Data are mean ± SEM; *n* = 3. *, Differs from control by P < 0.001 by Student's *t* test. (K) Reduced numbers of Geph+ postsynapses were detected in *col19a1*$^{-/-}$*::parv-cre::thy1-stop-yfp* mutant (KO) pfCTX compared with levels in control. Data are mean ± SEM; *n* = 3. *, Differs from control by P < 0.001 by Student's *t* test.

neurexin–neuroligin interactions; Waites et al., 2005). Significant differences in these mechanisms include the time scale at which they act and whether the action requires transcription and translation or the assembly of available synaptic machinery. To delineate between these mechanisms, we assessed the time scale required for mNC1 action in vitro. The minimal time required to see significant increases in Syt2+ puncta was 6 h, far too long for collagen XIX to be directly inducing the assembly of pregenerated synaptic components (Fig. 7, A–G). This result suggests that the NC1 domain of collagen XIX acts to prime inhibitory synaptogenesis by triggering the assembly of new synaptic components through transcription and translation. To test this hypothesis, we applied chemical blockers of transcription (i.e., actinomycin D and α-amanitin) and translation (cycloheximide) in conjunction with mNC1 peptides. In the presence of these inhibitors, the NC1 peptide was incapable of triggering nerve terminal assembly (Fig. 7, H–L). It is important to note, however, that collagen XIX does not appear to directly regulate *syt2* mRNA expression, since deletion of collagen XIX in vivo and application of NC1 fragments in vitro both failed to change *syt2* mRNA levels (Fig. 7, M and N).

Next, we addressed what receptors might mediate the synaptic priming affects of collagen XIX. Outside of the nervous system, matricryptins exert their influence by binding and signaling through a variety of RGD-dependent integrins (i.e., $\alpha_3\beta_1$, $\alpha_5\beta_1$, and $\alpha_v\beta_3$), even though some lack RGD sequences (Petitclerc et al., 2000; Ricard-Blum and Ballut, 2011; Oudart et al., 2015). The same is true at synapses: endostatin, the matricryptin derived from collagen XVIII, induces excitatory synapse assembly in inferior olivary neurons via $\alpha_3\beta_1$ integrins (Su et al., 2012). Here we tested whether the same was true for collagen XIX's NC1 domain. Indeed it is: the synaptogenic activity of the NC1 domain of collagen XIX is blocked by RGD peptides, indicating that integrins are involved in triggering inhibitory nerve terminal assembly in vitro (Fig. 8, A–D). These results are not entirely surprising given a recent article showing that NC1 signals through RGD-dependent integrins in cancer cells (Oudart et al., 2016). Further support for this notion stems from the discoveries that a variety of RGD-dependent integrins are present in cortical and synaptosome extracts and that Parv+ cells express β_1 (but not β_3) integrins (Fig. 8, E–G; and not depicted).

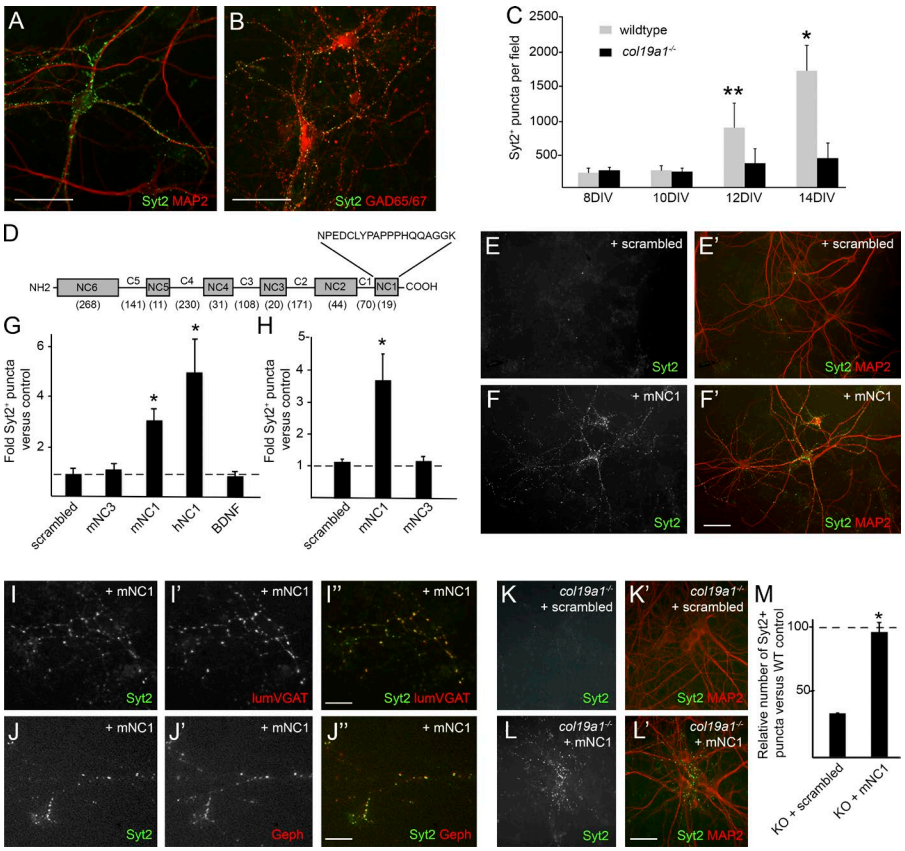

Figure 6. **Matricryptins derived from collagen XIX trigger inhibitory nerve terminal assembly.** (A) Syt2+ nerve terminals form on the somas and proximal dendrites of dissociated hippocampal neurons at DIV 14. Bar, 20 µm. (B) Syt2+ terminals that form in vitro are inhibitory terminals based on the coexpression of GAD isoforms. Bar, 20 µm. (C) Time course of the development of Syt2+ nerve terminals in vitro. The formation of Syt2+ nerve terminals is impaired in neurons isolated from *col19a1*$^{-/-}$ mutant mice. Data are mean ± SD; n = 4. * and **, Differs from all other conditions by $P < 0.05$ by Tukey–Kramer test for difference between means. (D) Schematic depiction of the domain structure of mouse collagen XIX. Collagenous (C) and noncollagenous (NC) domains are numbered beginning at the C terminus. The number of amino acids in each domain is shown in parentheses. The sequence of the NC1 domain is shown. (E and F) Mouse NC1 (mNC1) triggers Syt2+ terminal formation in HP neurons at DIV10. E and F depict Syt2-immunolabeling in HP cultures treated with Scrambled or mNC1 peptides; E′ and F′ depict merged overlays of Syt2 and MAP2 immunolabeling in these cultures. Bar, 20 µm. (G and H) Quantitation of mNC1-triggered Syt2+ puncta formation in both HP neurons (G) and CTX neurons (H) at DIV 10. Human NC1 peptides (hNC1) trigger an increase in Syt2+ puncta, but other collagen XIX peptides (i.e., mNC3) or neurotrophic factors (i.e., brain-derived neurotrophic factor) do not (G). Data are mean ± SEM; n = 4. *, Differs from controls, Scrambled, and NC3 peptides by $P < 0.001$ by Tukey–Kramer test for difference between means. (I) NC1-triggered Syt2+ puncta colabel with anti-lumVGAT, suggesting these puncta represent active synaptic sites. Bar, 10 µm. (J) Syt2+ puncta triggered by mNC1 colocalize with Geph. Bar, 10 µm. (K–L) Application of mNC1 rescues the loss of Syt2+ puncta in DIV12 HP neurons isolated from *col19a1*$^{-/-}$ mutant mice. K and L depict Syt2 immunolabeling; K′ and L′ depict merged overlays of Syt2 and MAP2 immunolabeling. Bar, 10 µm. (M) Quantitation of the number of Syt2+ puncta in *col19a1*$^{-/-}$ neuronal cultures treated with mNC1 or Scrambled peptides. Data are mean ± SEM; n = 3. *, Differs from Scrambled control in KO neurons by $P < 0.001$ by Tukey–Kramer test for difference between means.

These results raised the intriguing possibility that synaptogenic matricryptins derived from distinct collagens (i.e., endostatin from collagen XVIII and NC1 from collagen XIX) might be interchangeable in their ability to trigger synapse assembly through integrins. We tested this idea in dissociated inferior olivary neurons and the cortical culture systems described earlier. It turned out that each synaptogenic matricryptin had distinct activities: mNC1 was incapable of triggering VGluT2+ excitatory terminal formation in inferior olivary neurons, and endostatin was incapable of triggering Syt2+ inhibitory terminal formation in cortical cultures (Fig. 8, H–M).

This result suggests that the NC1 domain of collagen XIX requires an RGD-dependent integrin other than $\alpha_3\beta_1$. To confirm this hypothesis, we applied function-blocking antibodies directed against the α3 integrin subunit to dissociated neurons in conjunction with mNC1 peptides. Although this approach inhibited the synaptogenic activity of endostatin on inferior olivary neurons (Su et al., 2012), it did not block the action of mNC1 on cortical neurons (Fig. 8, N–Q). We therefore screened for other RGD-dependent integrins that may act as candidate receptors for collagen XIX. Our attention was drawn to $\alpha_5\beta_1$ integrin for several reasons. First, previous studies had demonstrated its presence in rodent CTX (Bi et al., 2001), and our analysis indicated it was expressed by neurons in our in vitro culture systems applied here (unpublished data). Second, we discovered that $\alpha_5\beta_1$ integrin was present in synaptosome fractions (Fig. 8 G). We therefore applied function blocking antibodies directed against the α_5 integrin subunit in conjunction with NC1 peptides and discovered that this blocked the ability of these peptides to trigger inhibitory nerve terminal assembly (Fig. 8, N–Q). Moreover, by covalently coupling NC1 fragments to beaded agarose, we were able to affinity-purify α_5 and β_1 integrins (but not α_v subunits) from cortical protein extracts (Fig. 8 R and not depicted), suggesting a direct interaction between NC1 and $\alpha_5\beta_1$ integrins.

Discussion

Whereas it is clear that Parv+ inhibitory synapses are essential for controlling the flow of neuronal activity, the mechanisms underlying the formation of these synapses are not well understood. Here we discovered that a neuronally expressed collagen contributes to the development of these synapses. Deletion of this collagen results in reduced numbers of inhibitory synapses, and specifically axosomatic inhibitory synapses, so it is not surprising that *col19a1*$^{-/-}$ mutant mice display a range a behavioral phenotypes, including neglect, impairment in sensorimotor gating, and seizures. It is surprising, however, that the majority of cells generating collagen XIX are not presynaptic Parv+ interneurons or their postsynaptic targets (Fig. S5 D). This suggests a novel paracrine mechanism that contributes to

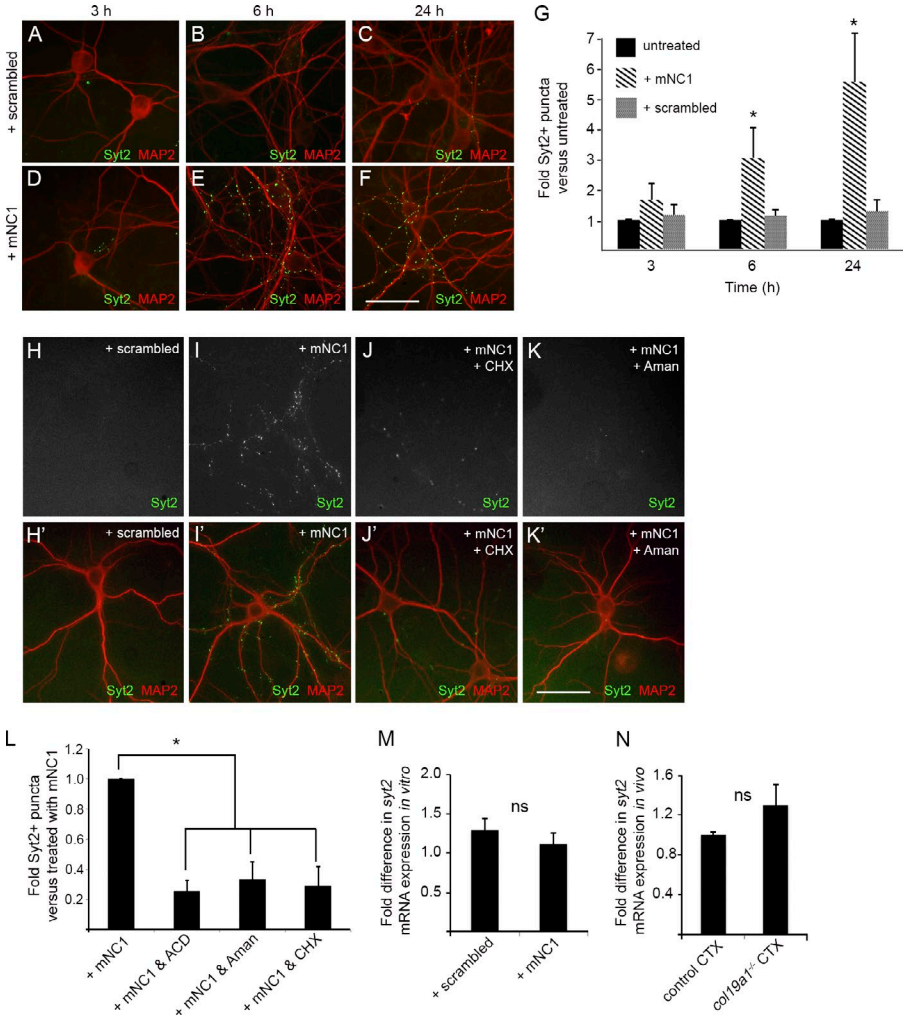

Figure 7. **Triggering of inhibitory nerve terminal formation by NC1 requires transcription and translation.** (A–F) Dissociated HP neurons were treated with mNC1 or Scrambled peptides for 3, 6, or 24 h. Bar, 50 µm. (G) Number of Syt2+ puncta in dissociated HP neurons treated with mNC1 or Scrambled peptides (or untreated) for 3, 6, or 24 h. Data are mean ± SEM; $n = 3$. *, Differs from untreated or Scrambled controls by $P < 0.01$ by Tukey–Kramer test for difference between means. (H–K) Dissociated HP neurons were treated with Scrambled peptides, mNC1, mNC1 + cyclohexamide (CHX), or mNC1 + α-amanitin (Aman). H–K depict Syt2 immunolabeling; H′–K′ depict merged overlay of Syt2 and MAP2 immunolabeling. Bar, 50 µm. (L) Number of Syt2+ puncta in dissociated HP neurons treated with mNC1, mNC1 + CHX, mNC1+ Aman, or mNC1 + actinomycin D (ACD). Data are mean ± SEM; $n = 3$. *, Differs from mNC1 treated neurons by $P < 0.01$ by Tukey–Kramer test for difference between means. (M) *syt2* mRNA levels in dissociated neurons treated with mNC1 or Scrambled peptides. Data are mean ± SEM; $n = 3$. ns, no statistical difference by Student's *t* test. (N) *syt2* mRNA levels in control and *col19a1*$^{-/-}$ CTX. Data are mean ± SEM; $n = 3$. ns, no statistical difference by Student's *t* test.

Parv+ inhibitory synapse formation and sheds new light on why patients with microdeletions in the genomic region encoding collagen XIX may suffer from schizophrenia (Liao et al., 2012).

As with any novel synaptogenic cue, an important question is how collagen XIX contributes to inhibitory synaptogenesis. Synaptogenesis is a multistep process, with unique sets of organizing cues required at each step (Scheiffele, 2003; Waites et al., 2005; Fox et al., 2007). Initially, growing axons from different brain regions must find and arborize in correct target fields, a process termed synaptic targeting. Correct targeting of pre- and postsynaptic partners does not immediately result in synaptic connections, and in some cases a significant temporal lag exists between the matching of appropriate synaptic partners and the formation of functional synapses (Lund, 1972). Transformation of nascent connections into functional synapses requires at least two steps: triggering each neuronal partner to transcribe, translate, and traffic key elements of pre- or postsynaptic machinery (a process called synaptic priming) and the subsequent, rapid assembly of these elements into functioning pre- and postsynaptic machineries (a process called synaptic induction; Waites et al., 2005). Based on its spatiotemporal expression pattern in CTX, the time course required for it to trigger presynaptic assembly in vitro, and the requirement of active transcription and translation for its synaptogenic activity, we posit that collagen XIX acts as a synaptic priming factor that may be diffusely localized in the developing cortex. In this sense, collagen XIX functions in a capacity similar to morphogens, growth factors, neurotrophins, and glial-derived matrix molecules (Hall et al., 2000; Alsina et al., 2001; Krylova et al., 2002; Ullian et al., 2004; Christopherson et al., 2005). Moreover, collagen XIX likely acts on inhibitory axons and terminals before postsynaptic inducers of presynaptic differentiation at these synapses, such as NCAM, Neuroligin 2, L1, and Slitrk3 (Graf et al., 2004; Guan and Maness, 2010; Takahashi et al., 2012; Woo et al., 2013; Liang et al., 2015; Maro et al., 2015; Tu et al., 2015). This may explain why inhibitory terminals initially form in the forebrain in the absence of some of these synaptic inducers, such as Neuroligin 2 (Gibson et al., 2009; Poulopoulos et al., 2009; Jedlicka et al., 2011; Liang et al., 2015; Babaev et al., 2016). Although our experiments suggest that matricryptins derived from collagen XIX are sufficient to trigger inhibitory nerve terminal assembly in vitro, the eventual loss of inhibitory synapses in the absence of Neuroligin 2 (Liang et al., 2015) suggests that collagen XIX is not sufficient for inhibitory synapse maintenance in vivo.

In many cases, priming and inductive synaptogenic cues are target derived, meaning that they are generated by the postsynaptic neurons at the synapse (Fox and Umemori, 2006). Target-derived matrix molecules, growth factors, and adhesion molecules all contribute to the formation of nerve terminals (Scheiffele et al., 2000; Umemori et al., 2004; Fox et al., 2007; Terauchi et al., 2010; Su et al., 2012). An interesting twist on results

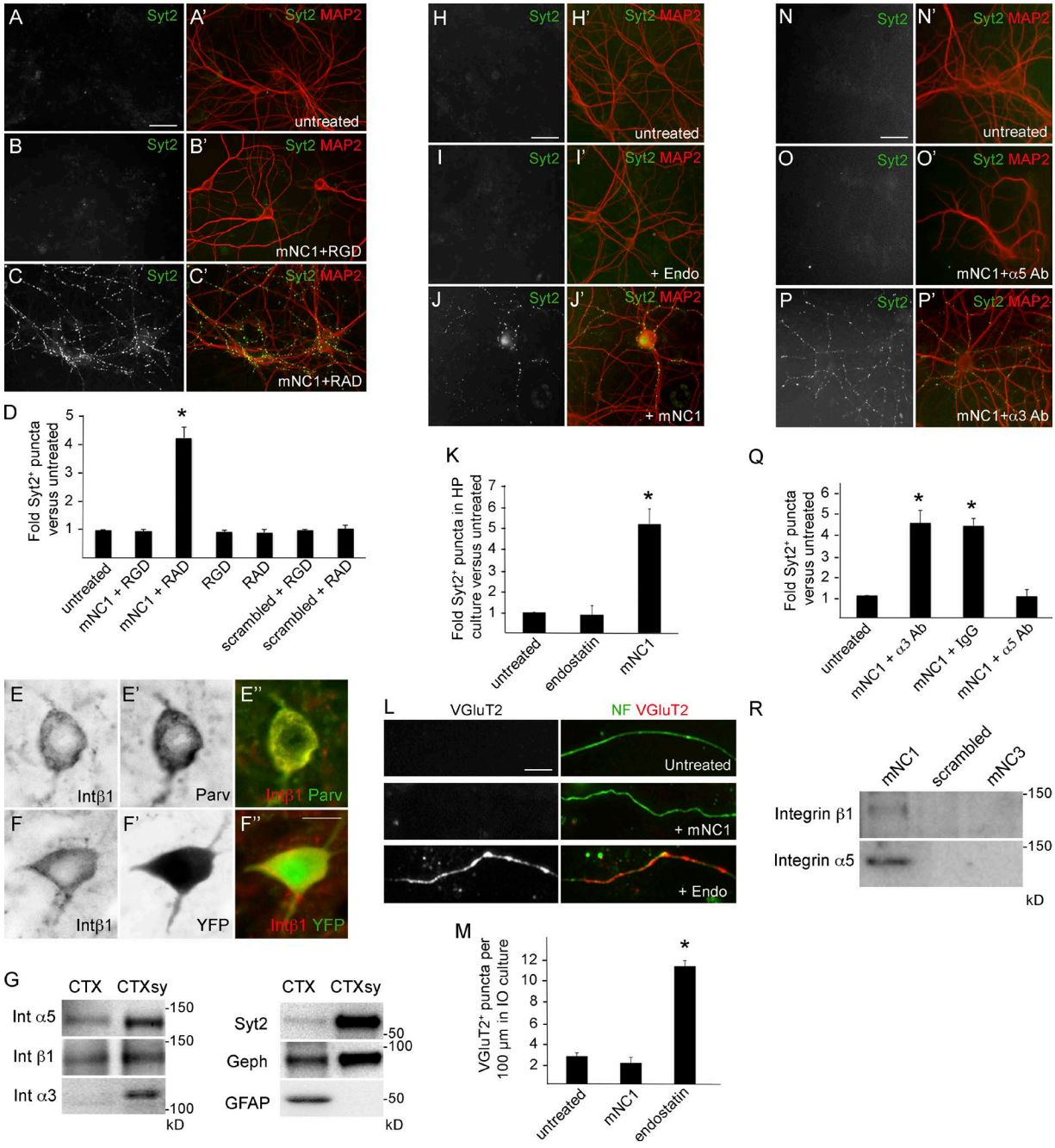

Figure 8. **NC1 signals through $\alpha_5\beta_1$ integrin to trigger nerve terminal formation.** (A–C) mNC1's ability to trigger the assembly of Syt2+ terminal puncta in HP neurons was inhibited by the application of 10 mM RGD peptides (B) but not control peptides (RAD; C). A, B, and C depict Syt2 immunolabeling; A′, B′, and C′ depict the merged overlay of Syt2 and MAP2 immunolabeling. Bar, 50 µm. (D) Quantitation of the number of Syt2+ puncta in HP cultures treated with combinations of mNC1, Scrambled, RAD, and RGD peptides. Data are mean ± SEM; $n = 3$. *, Differs from untreated neurons by $P < 0.01$ by Tukey–Kramer test for difference between means. (E and F) Parv+ interneurons (detected by Parv-IHC or transgenic expression of YFP in *parv-cre::thy1-stop-yfp* mice) are immunoreactive for integrin β_1. Bar, 12 µm. (G) Western blot of integrin subunits in total protein extracts and synaptosome fractions from CTX. The enrichment of synaptic proteins (i.e., Syt2, Geph) and the absence of GFAP demonstrate synaptosome purity. (H–J) Dissociated HP neurons treated with endostatin (Endo) or mNC1. Inhibitory terminals assessed by Syt2 immunolabeling. H–J depict Syt2 immunolabeling; H′–J′ depict merged overlay of Syt2 and MAP2 immunoreactivity. Bar, 50 µm. (K) Number of Syt2+ synaptic puncta induced by treatment in I–K. Data are mean ± SEM; $n = 3$. *, Differs from untreated neurons by $P < 0.01$ by Tukey–Kramer test for difference between means. (L) Dissociated inferior olivary neurons treated with Endo or mNC1. Excitatory nerve terminal assembly was assessed with VGluT2 immunolabeling. Axons were labeled with neurofilament (NF)-immunolabeling. Bar, 25 µm. (M) Number of VGluT2+ synaptic puncta induced by treatment in L. Data are mean ± SEM; $n = 3$. *, Differs from untreated neurons by $P < 0.01$ by Tukey–Kramer test for difference between means. (N–P) mNC1's ability to trigger the assembly of Syt2+ terminal puncta in HP neurons was inhibited by function blocking α_5 integrin antibodies (Ab; O) but not α_3 integrin antibodies (P). N–P depict Syt2 immunolabeling; N′–P′ depict the merged overlay of Syt2 and MAP2 immunolabeling. Bar, 50 µm. (Q) Number of Syt2+ puncta in HP cultures treated with combinations of mNC1 peptides, control antibodies, and integrin antibodies. Data are mean ± SEM; $n = 3$. *, Differs from untreated neurons by $P < 0.01$ by Tukey–Kramer test. (R) mNC1, Scrambled, and mNC3 peptides were immobilized to AffinityLink Plus coupling resin and incubated with CTX protein extracts. Elution fraction from mNC1-coupled resin contained α_5 and β_1 integrin subunits.

gathered here is that collagen XIX does not act as a target-derived synaptogenic cue, because the large majority of cells innervated by Parv+ interneurons do not generate *col19a1* mRNA. As such, collagen XIX likely acts in a paracrine fashion, more like glial-derived synaptogenic cues (Ullian et al., 2004; Christopherson et al., 2005; Kucukdereli et al., 2011). It is important to note that an alternative possibility is that the very small population of Parv+ interneurons that generate collagen XIX (<10%; Fig. 3) are capable of secreting collagen XIX to trigger the widespread formation of other Parv+ nerve terminals. This remains possible, but still would be classified as a paracrine mechanism of synaptogenesis. Future studies are needed to distinguish between these possibilities, but to our knowledge this remains the first article demonstrating interneurons participating in synapse formation in this fashion.

Finally, an important discovery in these studies is that a matricryptin released from collagen XIX by plasmin cleavage (Oudart et al., 2015) regulates inhibitory nerve terminal formation by signaling through integrins in vitro. In fact, many synaptogenic cues are activated or inactivated by proteolytic shedding, including agrin, collagens, SIRPα, and neuroligins (Reif et al., 2007; Matsumoto-Miyai et al., 2009; Peixoto et al., 2012; Su et al., 2012; Suzuki et al., 2012; Toth et al., 2013). Requirement of these posttranscriptional modifications in regulating the activity of synaptogenic cues allows for a rapid mechanism to turn these functions on or off in response to neuronal activity or other events in the developing brain. Unfortunately, at present we know little about the identity and role of matricryptin-releasing and ectodomain-shedding proteases at developing synapses. This will be an important gap to fill in future studies.

Materials and methods

Animals

CD1 and C57BL/6 mice were obtained from Charles River Laboratories. Collagen XIX–null mice (*col19a1*$^{-/-}$; previously referred to as N19) were generated by deleting the fourth exon of collagen XIX (Sumiyoshi et al., 2004). *Col19a1*$^{-/-}$ mutant mice were backcrossed for more than 10 generations on C57BL/6 mice. *Parv-cre*, *thy1-stop-yfp15*, *thy1-yfp (line H)*, and *reln*$^{rl/+}$ heterozygous mice were obtained from Jackson Labs (stock numbers 008069, 005630, 003782, and 000235, respectively). *Parv-cre* knock-in mice use the endogenous Parv promoter/enhancer elements to direct Cre recombinase expression, without disrupting Parv expression (Hippenmeyer et al., 2005). *Thy1-stop-yfp15* transgenic mice were generated to conditionally express enhanced YFP under the control of an exogenous Thy1 promoter (Buffelli et al., 2003); in the absence of Cre, expression of enhanced YFP in these mice is blocked by a loxP-flanked STOP fragment. *Thy1-yfp (line H)* transgenic mice were generated to express YFP under the control of an exogenous Thy1 promoter (Feng et al., 2000). Mice with a spontaneous mutation in the *reln* gene (*reln*$^{rl/rl}$; also called *reeler* mutant mice) were identified more than 60 years ago (Falconer, 1951). Recent studies have demonstrated that mice lacking a single copy of *reln* (*reln*$^{rl/+}$) display traits associated with complex brain disorders (Iafrati et al., 2014).

Genomic DNA was isolated from tails using the HotSHOT method, and genotyping was performed with the following primers: *lacz*, 5′-TTCACTGGCCGTCGTTTTACAACGTCGTGA-3′ and 5′-ATGTGAGCGAGTAACAACCCGTCGGATTCT-3′; *col19a1* (exon 4), 5′-CTTCGCAAAACGCATGCCTCAGA-3′ and 5′-TTGTTCGTTTGTTTGTTTTTAATCAATCAA-3′; *yfp*, 5′-AAGTTCATCTGCACCACCG-3′ and 5′-TCCTTGAAGAAGATGGTGCG-3′; and *cre*, 5′-TGCATGATCTCCGGTATTGA-3′ and 5′-CGTACTGACGGTGGGAGAAT-3′. The following primer pairs were used to genotype *reln*$^{rl/+}$ mice: 5′-TTAATCTGTCCTCACTCTGCCCTCT-3′ and 5′-GCAGACTCTCTTATTGTCTCTAC-3′; mutant *reln*, 5′-TTAATCTGTCCTCACTCTGCCCTCT-3′ and 5′-TTCCTCTCTTGCATCCTGTTTTG-3′ (Su et al., 2011). The following cycling conditions were used for *yfp*: 35 cycles using a denaturation temperature of 94°C for 30 s, annealing at 55°C for 1 min, and elongation at 72°C for 1 min. The following cycling conditions were used for *cre*: 35 cycles using a denaturation temperature of 95°C for 30 s, annealing at 52°C for 30 s, and elongation at 72°C for 45 s. The following cycling conditions were used for *col19a1*: 95°C for 5 min, followed by 35 cycles of amplification (95°C for 30 s, 52°C for 30 s, 72°C for 45 s), and 10 min at 72°C. All analyses conformed to National Institutes of Health guidelines and protocols and were approved by the Virginia Polytechnic Institute and State University Institutional Animal Care and Use Committees.

Reagents

All chemicals and reagents were obtained from Thermo Fisher Scientific or Sigma-Aldrich unless otherwise noted. All DNA primers were obtained from Integrated DNA Technologies.

Antibodies

The following antibodies were purchased: mouse anti-Syt2 (diluted 1:200 for IHC 1:100 for Western blot; Zebrafish International Resource Center; Fox and Sanes, 2007), rabbit anti-VGluT1 (diluted 1:500 for IHC; Synaptic Systems), mouse anti-VGluT1 (diluted 1:400 for Western blot; NeuroMab), rabbit anti-GAD65/67 (diluted 1:500 for IHC and 1:500 for Western blot; EMD Millipore), mouse anti-GAD67 (diluted 1:100 for IHC and 1:6,000 for Western blot; EMD Millipore), rabbit anti-MAP2 (diluted 1:1,000 for IHC; EMD Millipore), rabbit anti-Calbindin (diluted 1:2,500 for IHC; Swant), rabbit anti-Calretinin (diluted 1:1,000 for IHC; EMD Millipore), rabbit anti-somatostatin (diluted 1:250 for IHC; EMD Millipore), rabbit anti-GFAP (diluted 1:2,500 for IHC and 1:10,000 for Western blot; Dako), rabbit anti–Iba-1 (diluted 1:500 for IHC; Wako), rabbit anti-GFP (diluted 1:250 for IHC; Invitrogen), mouse anti-Gephyrin (diluted 1:500 for IHC and 1:1,000 for Western blot; Synaptic Systems), rabbit anti-lumVGAT (diluted 1:200 for live cell labeling; Synaptic Systems), mouse anti-actin (diluted 1:10,000 for Western blot; EMD Millipore), rabbit anti–integrin α_5 (diluted 1:1,000 for IHC and 1:3,000 for Western blot; EMD Millipore), rabbit anti–integrin α_3 (diluted 1:1,000 for IHC and 1:3,000 for Western blot; EMD Millipore), rat anti–integrin β_1 (diluted 1:500 for IHC and 1:1,000 for Western blot; EMD Millipore), and rabbit anti–integrin β_3 (diluted 1:1,000 for IHC and 1:2,000 for Western blot; Abcam). Fluorophore-conjugated secondary antibodies were obtained from Molecular Probes/Invitrogen and were applied at 1:1,000 dilutions.

Immunohistochemistry

Fluorescent IHC was performed on 16-µm cryosectioned PFA-fixed brain tissue or cultured neurons (Fox et al., 2007; Su et al., 2010, 2012). Tissue slides were allowed to air-dry for 15 min before being incubated with blocking buffer (2.5% normal goat serum, 2.5% BSA, and 0.1% Triton X-100 in PBS) for 30 min. Primary antibodies were diluted in blocking buffer and incubated on tissue sections overnight at 4°C. On the next day, tissue slides were washed in PBS, and secondary antibodies diluted 1:1,000 in blocking buffer were applied to slides for 1 h at RT.

After thorough washes in PBS, tissue slides were coverslipped with VectaShield (Vector Laboratories). Images of in vitro assays were acquired on an Axio Imager A2 fluorescent microscope (ZEISS) equipped with a 20× air Plan-Apochromat objective (NA 0.8; ZEISS)

and a AxioCam MRm (ZEISS). Images of tissue were acquired on a confocal microscope (LSM 700; ZEISS) equipped with a 20× air Plan-Apochromat objective (NA 0.8; ZEISS) and a 40× oil EC Plan-NeoFluar objective (NA 1.3; ZEISS). When comparing different ages of tissues or between genotypes, images were acquired with identical parameters, and similar gamma adjustments were made to age-matched mutant and control images in Adobe Photoshop or ImageJ. A minimum of three animals (per genotype and per age) were compared in all IHC experiments. Mean fluorescent intensities and area coverage of IHC images were measured in ImageJ (Singh et al., 2012). For quantification of axosomatic synapses, single optical sections of confocal images were analyzed, and the density of synaptic elements ($Syt2^+$ or $Geph^+$ puncta) was quantified per unit length of the cell surface in ImageJ.

In situ hybridization

In situ hybridization (ISH) was performed on 16-µm sagittal cryosectioned tissues (Su et al., 2010, 2011, 2012). Antisense riboprobe generation of full-length *col19a1* (EMM1002-97504659) and *syt1* (MM1013-9199901) were from Open Biosystems. An 800-bp fragment of *parv* (corresponding to nt 2–825) was PCR-cloned into pGEM Easy T vector (Promega) with the following primers: 5′-TCTGCTCATCCA AGTTGCAG-3′ and 5′-TCCTGAAGGACTCAACCCC-3′. In brief, riboprobes were synthesized using digoxigenin-labeled UTP (Roche) and the MAXIscript In Vitro Transcription kit (Ambion). Probes were hydrolyzed to 500 nt. Sagittal brain sections were prepared. Tissue sections were fixed in 4% PFA for 10 min, washed with DEPC-PBS three times, and incubated in proteinase K solution (1 µg/ml proteinase K, 50 mM Tris, pH 7.5, and 5 mM EDTA) for 10 min. Subsequently, slides were washed with DEPC-PBS, fixed with 4% PFA for 5 min, washed with DEPC-PBS, and incubated in acetylation buffer (1.33% triethanolamine, 20 mM HCl, and 0.25% acetic anhydride) for 10 min. Slides were then permeabilized in 1% Triton X-100 for 30 min and washed with DEPC-PBS. Endogenous peroxidase was blocked by incubation in 0.3% H_2O_2 for 30 min. Tissue sections were equilibrated in hybridization buffer (1× prehybridization, 0.1 mg/ml yeast tRNA, 0.05 mg/ml heparin, and 50% formamide) for 1 h and incubated with probes at 65°C overnight (Su et al., 2010). After washing in 0.2× SSC at 65°C, bound riboprobes were detected by HRP–conjugated anti-digoxigenin antibodies and fluorescent staining with Tyramide Signal Amplification (TSA) systems (PerkinElmer). After mounting sections in VectaShield, images were obtained on a ZEISS LSM 700 confocal microscope equipped with a 20× air Plan-Apochromat objective (NA 0.8). A minimum of three animals per genotype and age were compared in ISH experiments.

Quantitative real-time PCR

RNA was isolated using the BioRad Total RNA Extraction from Fibrous and Fatty Tissue kit (BioRad). cDNAs were generated from 200 ng RNA with the Superscript II Reverse Transcription First Strand cDNA Synthesis kit (Invitrogen). Quantitative real-time PCR (qPCR) was performed on a Chromo 4 Four Color Real-Time system (BioRad) using iQ SYBRGreen Supermix (BioRad; Su et al., 2010). *Col19a1* primers for qPCR were 5′-ATTGGACATAAGGGCGACAA-3′ and 5′-AGTCTCCTTTGGCTCCTGGT-3′. *Gapdh* primers for qPCR were 5′-CGTCCCGTAGACAAAATGGT-3′ and 5′-TTGATGGCAACA ATCTCCAC-3′. *Syt2* primers for qPCR were 5′-CTGCCTGGTTTA CAGAGCAA-3′ and 5′-TGTTTCTCATGGTGGCAGAG-3′. qPCR primers were designed over introns. The following cycling conditions were used with 10 ng RNA: 95°C for 30 s, followed by 40 cycles of amplification (95°C for 5 s, 60°C for 30 s, 55°C for 60 s, read plate) and a melting curve analysis. Relative quantities of RNA were determined using the ΔΔ−CT method. A minimum of $n = 3$ experiments (each in triplicate) was run for each gene, at each age examined. To be considered differentially expressed, genes had to be twofold higher in the averaged sample sets ($n = 3$, $P < 0.05$). Each individual run included separate GAPDH control reactions.

Western blot and synaptosome purification

Mouse brains were perfused with PBS, and tissue was dissected in ice-cold PBS and lysed in modified loading buffer containing 50 mmol/l Tris-HCl, pH 6.8, 2% sodium dodecyl sulfate (SDS), 10% glycerol, and protease inhibitors (1 mmol/l PMSF). Cortical synaptosome fractions were prepared as follows (Fox and Sanes, 2007; Su et al., 2012): cortex was dissected from P28–P35 mice and homogenized in solution A (0.32 M sucrose, 1 mM $NaHCO_3$, 1 mM $MgCl_2$, and 0.5 mM $CaCl_2$). Homogenate was filtered through cheesecloth, and the resulting solution was centrifuged for 10 min at 1475 *g*. Pelleted material was washed with solution A, rehomogenized in solution A, centrifuged for 10 min at 755 *g*, and combined with the supernatant from the first centrifugation. The resulting solution was centrifuged for 10 min at 755 *g*. Pelleted material was discarded. The supernatant was then centrifuged for 10 min at 17,300 *g*. Pelleted material was resuspended in solution A, homogenized, and centrifuged for 10 min. Pelleted material was resuspended in solution B (0.32 M sucrose and 1 mM $NaHCO_3$) and centrifuged in a sucrose density gradient (1.2, 1.0, and 0.85 M sucrose with 1 mM $NaHCO_3$) for 2 h at 100,000 *g*. Material was collected between the 1.0- and 1.2-M sucrose gradients. This material was resuspended in solution B and centrifuged for 20 min at 48,200 *g*. After centrifugation, the supernatant was discarded, and the pelleted material was resuspended in lysing buffer (6 mM Tris-HCl, pH 8.1). The resulting suspension was stirred for 45 min at 4°C and then centrifuged for 20 min at 48,200 *g*. Pelleted material was again resuspended in solution B, homogenized, and centrifuged in a sucrose density gradient for 2 h at 100,000 *g*. Material collected between the 1.0- and 1.2-M sucrose bands was diluted with solution B and centrifuged for 20 min at 48,200 *g*. The resulting pellet contained the synaptosome fraction and was suspended in solution B with protease inhibitors (1 µg/ml pepstatin A, 2 µg/ml leupeptin, 1.6 µg/ml aprotinin, 200 µM PMSF, 0.1 mg/ml benzamide, and 8 µg/ml calpain inhibitor II).

For Western blot analysis, equal amounts of protein were loaded and separated by SDS-PAGE and transferred to PVDF membrane (Su et al., 2010, 2012). After blocking in 5% nonfat milk in PBS (containing 0.05% Tween-20), PVDF membranes were incubated with appropriate primary antibodies, followed by HRP-conjugated secondary antibodies. Immunoblotted proteins were detected with an enhanced chemiluminescent detection system (ECL Plus, Amersham Pharmacia Biotech).

Neuronal culture

Hippocampal or cortical tissues were dissected from P0 mouse brains and digested in 0.25% trypsin (Brooks et al., 2013). Trypsin was inactivated, and tissue was transferred to neurobasal medium containing 0.5 mM L-glutamine, 25 mM L-glutamate, 10 µg/ml gentamicin, and B27 supplement. Single-cell suspensions were plated on poly-L-lysine–treated chamber slides and cultured for 4 d. After 4–6 additional days in neurobasal medium containing 0.5 mM L-glutamine, 10 mg/ml gentamicin, and B27 supplement, hippocampal or cortical neurons were treated with mouse collagen XIX NC1 (mNC1; 0.2 µg/ml; GenScript), NC3 (0.2 µg/ml; GenScript), Scrambled (0.2 µg/ml; GenScript), human collagen XIX NC1 (hNC1; 0.2 µg/ml; GenScript), brain-derived neurotrophic factor (50 ng/ml), and endostatin (0.1 mg/ml; ProSpec) alone or combined with RGD (10 mM; Sigma-Aldrich), RAD (10 mM; Sigma-Aldrich), rabbit anti–integrin α_5 (25 µg/ml; EMD Millipore), rabbit anti–integrin α_3 (25 µg/ml; EMD Millipore), and/or mouse immunoglobulin G (25 µg/ml), cycloheximide (10 µg/ml;

Sigma-Aldrich), α-amanitin (5 µg/ml; Sigma-Aldrich), and actinomycin D (0.2 µg/ml; Sigma-Aldrich). After 1–2 d, cells were fixed with 4% PFA (in PBS), permeabilized with 0.5% Triton X-100, and immunostained. Importantly, WT cultures were treated with these reagents and peptides at 8–9 days in vitro (DIV), whereas cultures from *col19a1*$^{-/-}$ mutants were treated at DIV 10–11. Data analysis of hippocampal or cortical cultures is based on the total number of Syt2^{+} puncta in each visual area and normalized to untreated controls. Fields imaged were selected based on similar densities of neuronal cell bodies and dendrites from MAP2 immunoreactivity (and blind to Syt2 immunolabeling). Images were obtained with an Axio Imager A2 fluorescent microscope equipped with a 20× air Plan-Apochromat objective (NA 0.8) and an AxioCam MRm.

Cultures of inferior olivary neurons were generated from P0 CD1 mouse brains. Inferior olives were dissected and incubated in 0.25% trypsin at 37°C for 15 min. After digestion, soybean trypsin inhibitor was used to inactivate the trypsin, and inferior olive tissues were transferred to 3G medium (neurobasal medium with 0.5 mM L-glutamine, 25 µM L-glutamate, 10 µg/ml gentamicin, and 10% FBS). A single-cell suspension was generated by triturating tissues through a 1,000-µl pipet tip. 10^5 cells were added to each well of a poly-L-lysine–treated eight-well laboratory-Tek chamber slide. Cultures were incubated at 37°C, 5% CO_2 for 4 d, and then medium was changed to 2G medium (neurobasal medium with 0.5 mM L-glutamine, 10 µg/ml gentamicin, and B27) for at least another 2 d. After 6 DIV, cells were treated with endostatin (0.1 µg/ml) or mNC1 (0.2 µg/ml) for an additional 2 d. Cells were then fixed with 4% PFA (in PBS), permeabilized with 0.5% Triton X-100, and immunostained. Images were obtained with an Axio Imager A2 fluorescent microscope equipped with a 20× air Plan-Apochromat objective (NA 0.8) and an AxioCam MRm and were quantified in ImageJ.

Live labeling of inhibitory synapses with lumVGAT antibodies

LumVGAT antibody labeling was performed to label active presynaptic nerve terminals (Martens et al., 2008). On DIV 11 (and 2 d after mCN1 treatment), primary hippocampal neurons were incubated in modified Krebs-Ringer solution (119 mM NaCl, 55 mM KCl, 1.0 mM NaH_2PO_4, 2.5 mM $CaCl_2$, 1.3 mM $MgCl_2$, 20 mM Hepes, and 11 mM D-glucose) and rabbit anti-lumVGAT (5 µg/ml) at 37°C for 5 min, followed by two washes with modified Krebs-Ringer solution and one wash with PBS. Neurons were subsequently fixed and immunostained as described earlier.

AminoLink Plus coupling assay

NC1 integrin binding was assessed by conjugating NC1 peptides with AminoLink Plus coupling resin (ThermoFisher Scientific). 0.4 mg collagen XIX NC1-, NC3-, or NC1-Scrambled peptide was dissolved in coupling buffer (0.1 M sodium phosphate and 0.15 M NaCl, pH 7.2) and conjugated with AminoLink Plus resin. Cyanoborohydride solution (5 M $NaCNBH_3$ in 1 M NaOH) was added and incubated overnight at 4°C. After serial washing with coupling buffer, quenching buffer (1 M Tris-HCl, pH 7.4), wash solution (1 M NaCl), and binding buffer (50 mM Tris-HCl, pH 7.6, 150 mM NaCl, 2 mM EDTA, pH 8.0, 1% Triton X-100, and 50 mM NaF), cortical protein extracts (from P15 WT brains lysed in binding buffer) were incubated in the column overnight at 4°C. After washing with binding buffer, bound proteins were eluted in 1% SDS buffer. Eluted samples were precipitated with 15% trichloroacetic acid on ice, pelleted by centrifugation, and resuspended in lysate buffer (80 mM Tris-HCl, pH 6.8, 2% SDS, and 10% glycerol). Eluted protein was analyzed by Western blot.

Bioinformatic analysis

The EvoCor platform was used to predict mouse genes functionally related to *col19a1*, *col18a1*, *col4a3*, and *col4a6* using evolutionary history and correlated gene expression profiles. The EvoCor platform is freely available at http://pilot-hmm.vbi.vt.edu/. The Allen Brain Atlas (http://mouse.brain-map.org) and PubMed (http://www.ncbi.nlm.nih.gov/pubmed) were used to assess the expression pattern and known functions of the top 40 functionally related candidates identified by EvoCor analysis.

Behavioral analyses

PPI assay. PPI tests were conducted in SR-LAB acoustic startle chambers (San Diego Instruments) based on previously described methods (Geyer and Dulawa, 2003) with slight modifications. The background noise was 65 dB, and the prepulse (pp) was 120 dB (pp120) with 40-ms duration. In each startle trail, a 20 ms prepulse at 69 dB (pp4), 73 dB (pp8), or 81 dB (pp16) was followed by a 40-ms startle pulse at 120 dB. A total of 64 electrical signal readings were recorded at 1-ms intervals during each assay. The percentage PPI was calculated by using the following equation: % PPI = 100 × (score of 120 dB pulse alone – score of prepulse [pp4, pp8, or pp16])/(score of 120 dB pulse alone). We analyzed 27 WT mice and 39 collagen XIX–deficient mutant mice. All mice were 3–5 mo old. Importantly, if a mouse was observed to have a seizure during the assay, or any other behavioral assay, the data from that mouse were not included in the data analysis.

Nest-building assay. Approximately 1 h before the dark phase, mice were transferred into clean cages and housed in isolation. One cotton nestlet was added in the same location of each cage. Each cotton nestlet weighed ∼2.8 g at the onset of the experiment. The next morning, we assessed the nests in two ways. First, we visually scored each nest with a rating scale of 1–5 (1, >90% of the cotton nestlet remained intact; 2, 50–90% of the cotton nestlet remained intact; 3, 50–90% of the nestlet was shredded; 4, >90% was shredded but the nest was not complete; 5, >90% was torn and the nest was complete; Deacon, 2006). Second, we weighed the portions of each nestlet that remained unused (which included any fragments weighing >0.1 g). All mice analyzed were 3–5 mo old. Data presented were obtained from 21 WT mice and 25 collagen XIX–deficient mutant mice. Each mouse was assayed once per week, and this was repeated for three consecutive weeks.

Open-field assay. Open-field assays (Dulawa et al., 2004) were performed in 40 × 40-cm plastic boxes with black walls. The center of the open field was defined as the central area 10 cm away from any wall. The environment illumination was at ∼200 lux. After each mouse was placed into the open field apparatus, its movement was recorded for 60 min with overhead cameras. Movement was tracked and analyzed with ANY-maze version 4.99 tracking system (Stoelting Co.). Data presented were obtained from 29 WT mice and 42 collagen XIX–deficient mutant mice. All mice were 3–5 mo old.

Crawley sociability and social novelty preference assay. The Crawley sociability and social novelty preference assay (Kaidanovich-Beilin et al., 2011) was performed in a standard three-chamber box, with an open middle chamber that allows free access to each of the flanking chambers (Stoelting). The test mouse was habituated in the middle chamber for 5 min, and a novel conspecific male was placed inside a wire containment cup in one side chamber. The duration of contacts between the subject and either the empty housing or the housing containing the novel conspecific was recorded by three video cameras. A single 10-min session was performed for each subject. Social memory was immediately tested by placing a new, novel conspecific male in the empty chamber and leaving the previous (now familiar) conspecific in place. For 10 min, the duration of contacts between the subject and either the novel conspecific or the familiar conspecific was recorded. StreamPix5 was used to analyze the data. 15 WT male mice and 25 collagen XIX–deficient mutant male mice were used. All mice were 3–5 mo old.

Rotarod

Standard rotarod experiments were performed on a Rota-Rod with a 3-cm rod (UGO Basile; Su et al., 2012). At the onset of experiments, rods rotated at 1 rpm; however, every 15 s, the speed increased by 1 rpm. The Rota-Rod recorded the time at which each mouse fell. A total of 20 mutants and 19 littermate controls were analyzed. All mice were 3–5 mo old.

Wheel running activity assay

Wheel running activity was monitored in wheel cages from Lafayette Instruments. A magnetic switch located on the wheel recorded each revolution as an event and sent that information to a compatible computer in 5-min bins using ClockLab software R2011b. Each mouse was placed in a separate cage and put on cart randomly. All mice were housed in a standard animal maintenance facility under a 12 h light/12 h dark cycle. Mice were habituated for 2 d before continually recording activity for 2 wk. A total of 8 collagen XIX–deficient mutant mice and 10 littermate WT mice were analyzed.

EEG/EMG recordings

Unless specifically noted, all EEG/EMG hardware and software were from Pinnacle Technologies. WT, *col19a1*$^{-/-}$ mutant mice, and *reln*$^{rl/+}$ heterozygous mice were anesthetized with ketamine, the skull was exposed, and EEG/EMG headmounts were affixed to the skull with four recording electrode screws, ensuring that all four screws were implanted into the skull overlying the motor or sensory cortex in each cerebral hemisphere. EMG leads were implanted into nuchal muscles of the dorsal neck. The skull was then encased in a thick layer of dental acrylic (US Dental Depot) to prevent detachment of the headmount and EMG leads. Mice were rested for 5 d and then were tethered to the EEG/EMG recording chamber by connecting a 100× preamplifier containing a 1.0-Hz high-pass EEG filter and a 10-Hz high-pass EMG filter into the ports of the headmount. Mice remained tethered for 2–3 d before recording commenced, and EEG/EMG data were recorded for 5 d in normal light/dark phase. EEG and EMG activity was recorded using Sirenia Acquisition software, and data acquisition was performed at a sampling rate of 10,000 Hz. Spontaneous seizures and spikes in EEG/EMG activity were identified and analyzed with Sirenia Seizure software. Generalized motor seizures were identified as high-amplitude, high-frequency neural and muscular activity that persisted for longer than 30 s. A total of 14 *col19a1*$^{-/-}$ mutant mice, 2 *reln*$^{rl/+}$ heterozygotes, and 9 WT mice were analyzed in these studies.

PTZ-induced seizures

To assess responses to drug-induced seizures, mice were injected with PTZ (40 µg/kg in 0.2 ml PBS) and then visually monitored while blind to EEG/EMG recordings for 15 min. Seizures were scored manually every minute after with the following scoring criteria: 0, normal activity; 1, reduced motility and prostate position; 2, partial clonus; 3, generalized clonus; 4, tonic-clonic seizure; and 5, death. To ensure that surgical implantation of EEG/EMG did not induce altered response to administration of PTZ in mutants, all data presented in Fig. 2 E were obtained from *col19a1*$^{-/-}$ mutant mice and littermate WT mice that did not have electrodes implanted (n = 7 WT mice and 10 *col19a1*$^{-/-}$ mutant mice).

Online supplemental material

Fig. S1 provides bioinformatic analysis of other synaptogenic collagen genes with EvoCor. Fig. S2 shows that loss of collagen XIX leads to impaired inhibitory synapse formation. Fig. S3 shows that Syt2^{+} terminals originate from Parv^{+} GABAergic interneurons in cortex and HP. Fig. S4 demonstrates that the loss of collagen XIX does not alter the number or distribution of Parv^{+} or *syt2*$^{+}$ interneurons. Fig. S5 reveals that the in vitro application of mNC1 triggers an increase in GAD67^{+} puncta. Online supplemental material is available at http://www.jcb.org/cgi/content/full/jcb.201509085/DC1.

Acknowledgments

We thank Dr. G. Valdez, Virginia Tech Carilion Research Institute (VTC RI), for assistance with EvoCor analysis; Dr. K. Mukherjee (VTCRI) for assistance with AminoLink coupling; Dr. A. Morozov (VTCRI) and Dr. W. Ito (VTCRI) for assistance with behavioral analysis; Dr. F. Ramirez (Icahn School of Medicine) for *col19a1*$^{-/-}$ mice; and L. Dahora for technical assistance.

This work was supported in part by a Brain and Behavior Research Foundation NARSAD Independent Investigator Award (M.A. Fox), National Institutes of Health grant EY021222 (M.A. Fox), and a Virginia Tech Carilion Research Institute Medical Research Scholar fellowship (A. Monavarfeshani).

The authors declare no competing financial interests.

Submitted: 21 September 2015
Accepted: 11 February 2016

References

Ackley, B.D., J.R. Crew, H. Elamaa, T. Pihlajaniemi, C.J. Kuo, and J.M. Kramer. 2001. The NC1/endostatin domain of *Caenorhabditis elegans* type XVIII collagen affects cell migration and axon guidance. *J. Cell Biol.* 152:1219–1232. http://dx.doi.org/10.1083/jcb.152.6.1219

Albrecht, A., and O. Stork. 2012. Are NCAM deficient mice an animal model for schizophrenia? *Front. Behav. Neurosci.* 6:43. http://dx.doi.org/10.3389/fnbeh.2012.00043

Alsina, B., T. Vu, and S. Cohen-Cory. 2001. Visualizing synapse formation in arborizing optic axons in vivo: dynamics and modulation by BDNF. *Nat. Neurosci.* 4:1093–1101. http://dx.doi.org/10.1038/nn735

Babaev, O., P. Botta, E. Meyer, C. Müller, H. Ehrenreich, N. Brose, A. Lüthi, and D. Krueger-Burg. 2016. Neuroligin 2 deletion alters inhibitory synapse function and anxiety-associated neuronal activation in the amygdala. *Neuropharmacology.* 100:56–65. http://dx.doi.org/10.1016/j.neuropharm.2015.06.016

Belforte, J.E., V. Zsiros, E.R. Sklar, Z. Jiang, G. Yu, Y. Li, E.M. Quinlan, and K. Nakazawa. 2010. Postnatal NMDA receptor ablation in corticolimbic interneurons confers schizophrenia-like phenotypes. *Nat. Neurosci.* 13:76–83. http://dx.doi.org/10.1038/nn.2447

Benes, F.M., and S. Berretta. 2001. GABAergic interneurons: implications for understanding schizophrenia and bipolar disorder. *Neuropsychopharmacology.* 25:1–27. http://dx.doi.org/10.1016/S0893-133X(01)00225-1

Bi, X., G. Lynch, J. Zhou, and C.M. Gall. 2001. Polarized distribution of alpha5 integrin in dendrites of hippocampal and cortical neurons. *J. Comp. Neurol.* 435:184–193. http://dx.doi.org/10.1002/cne.1201

Brooks, J.M., J. Su, C. Levy, J.S. Wang, T.A. Seabrook, W. Guido, and M.A. Fox. 2013. A molecular mechanism regulating the timing of corticogeniculate innervation. *Cell Reports.* 5:573–581. http://dx.doi.org/10.1016/j.celrep.2013.09.041

Buffelli, M., R.W. Burgess, G. Feng, C.G. Lobe, J.W. Lichtman, and J.R. Sanes. 2003. Genetic evidence that relative synaptic efficacy biases the outcome of synaptic competition. *Nature.* 424:430–434. http://dx.doi.org/10.1038/nature01844

Castorina, A., A.G. D'Amico, S. Scuderi, G.M. Leggio, F. Drago, and V. D'Agata. 2013. Dopamine D3 receptor deletion increases tissue plasminogen activator (tPA) activity in prefrontal cortex and hippocampus. *Neuroscience.* 250:546–556. http://dx.doi.org/10.1016/j.neuroscience.2013.07.053

Christopherson, K.S., E.M. Ullian, C.C. Stokes, C.E. Mullowney, J.W. Hell, A. Agah, J. Lawler, D.F. Mosher, P. Bornstein, and B.A. Barres. 2005. Thrombospondins are astrocyte-secreted proteins that promote CNS synaptogenesis. *Cell.* 120:421–433. http://dx.doi.org/10.1016/j.cell.2004.12.020

Deacon, R.M. 2006. Assessing nest building in mice. *Nat. Protoc.* 1:1117–1119. http://dx.doi.org/10.1038/nprot.2006.170

Dittmar, W.J., L. McIver, P. Michalak, H.R. Garner, and G. Valdez. 2014. EvoCor: a platform for predicting functionally related genes using phylogenetic and expression profiles. *Nucleic Acids Res.* 42(W1):W72-5. http://dx.doi.org/10.1093/nar/gku442

Dulawa, S.C., K.A. Holick, B. Gundersen, and R. Hen. 2004. Effects of chronic fluoxetine in animal models of anxiety and depression. *Neuropsychopharmacology.* 29:1321–1330. http://dx.doi.org/10.1038/sj.npp.1300433

Falconer, D.S. 1951. Two new mutants, 'trembler' and 'reeler', with neurological actions in the house mouse (*Mus musculus* L.). *J. Genet.* 50:192–201. http://dx.doi.org/10.1007/BF02996215

Feng, G., R.H. Mellor, M. Bernstein, C. Keller-Peck, Q.T. Nguyen, M. Wallace, J.M. Nerbonne, J.W. Lichtman, and J.R. Sanes. 2000. Imaging neuronal subsets in transgenic mice expressing multiple spectral variants of GFP. *Neuron.* 28:41–51. http://dx.doi.org/10.1016/S0896-6273(00)00084-2

Fox, M.A., and J.R. Sanes. 2007. Synaptotagmin I and II are present in distinct subsets of central synapses. *J. Comp. Neurol.* 503:280–296. http://dx.doi.org/10.1002/cne.21381

Fox, M.A., and H. Umemori. 2006. Seeking long-term relationship: axon and target communicate to organize synaptic differentiation. *J. Neurochem.* 97:1215–1231. http://dx.doi.org/10.1111/j.1471-4159.2006.03834.x

Fox, M.A., J.R. Sanes, D.B. Borza, V.P. Eswarakumar, R. Fässler, B.G. Hudson, S.W. John, Y. Ninomiya, V. Pedchenko, S.L. Pfaff, et al. 2007. Distinct target-derived signals organize formation, maturation, and maintenance of motor nerve terminals. *Cell.* 129:179–193. http://dx.doi.org/10.1016/j.cell.2007.02.035

Geyer, M.A., and S.C. Dulawa. 2003. Assessment of murine startle reactivity, prepulse inhibition, and habituation. Curr Protoc. Neurosci. Chapter 8:Unit 8.17.

Gibson, J.R., K.M. Huber, and T.C. Südhof. 2009. Neuroligin-2 deletion selectively decreases inhibitory synaptic transmission originating from fast-spiking but not from somatostatin-positive interneurons. *J. Neurosci.* 29:13883–13897. http://dx.doi.org/10.1523/JNEUROSCI.2457-09.2009

Gonzalez-Burgos, G., and D.A. Lewis. 2012. NMDA receptor hypofunction, parvalbumin-positive neurons, and cortical gamma oscillations in schizophrenia. *Schizophr. Bull.* 38:950–957. http://dx.doi.org/10.1093/schbul/sbs010

Gonzalez-Burgos, G., T. Hashimoto, and D.A. Lewis. 2010. Alterations of cortical GABA neurons and network oscillations in schizophrenia. *Curr. Psychiatry Rep.* 12:335–344. http://dx.doi.org/10.1007/s11920-010-0124-8

Gonzalez-Burgos, G., K.N. Fish, and D.A. Lewis. 2011. GABA neuron alterations, cortical circuit dysfunction and cognitive deficits in schizophrenia. *Neural Plast.* 2011:723184. http://dx.doi.org/10.1155/2011/723184

Graf, E.R., X. Zhang, S.X. Jin, M.W. Linhoff, and A.M. Craig. 2004. Neurexins induce differentiation of GABA and glutamate postsynaptic specializations via neuroligins. *Cell.* 119:1013–1026. http://dx.doi.org/10.1016/j.cell.2004.11.035

Guan, H., and P.F. Maness. 2010. Perisomatic GABAergic innervation in prefrontal cortex is regulated by ankyrin interaction with the L1 cell adhesion molecule. *Cereb. Cortex.* 20:2684–2693. http://dx.doi.org/10.1093/cercor/bhq016

Hall, A.C., F.R. Lucas, and P.C. Salinas. 2000. Axonal remodeling and synaptic differentiation in the cerebellum is regulated by WNT-7a signaling. *Cell.* 100:525–535. http://dx.doi.org/10.1016/S0092-8674(00)80689-3

Hippenmeyer, S., E. Vrieseling, M. Sigrist, T. Portmann, C. Laengle, D.R. Ladle, and S. Arber. 2005. A developmental switch in the response of DRG neurons to ETS transcription factor signaling. *PLoS Biol.* 3:e159. http://dx.doi.org/10.1371/journal.pbio.0030159

Hunt, R.F., K.M. Girskis, J.L. Rubenstein, A. Alvarez-Buylla, and S.C. Baraban. 2013. GABA progenitors grafted into the adult epileptic brain control seizures and abnormal behavior. *Nat. Neurosci.* 16:692–697. http://dx.doi.org/10.1038/nn.3392

Iafrati, J., M.J. Orejarena, O. Lassalle, L. Bouamrane, C. Gonzalez-Campo, and P. Chavis. 2014. Reelin, an extracellular matrix protein linked to early onset psychiatric diseases, drives postnatal development of the prefrontal cortex via GluN2B-NMDARs and the mTOR pathway. *Mol. Psychiatry.* 19:417–426. http://dx.doi.org/10.1038/mp.2013.66

Jedlicka, P., M. Hoon, T. Papadopoulos, A. Vlachos, R. Winkels, A. Poulopoulos, H. Betz, T. Deller, N. Brose, F. Varoqueaux, and S.W. Schwarzacher. 2011. Increased dentate gyrus excitability in neuroligin-2-deficient mice in vivo. *Cereb. Cortex.* 21:357–367. http://dx.doi.org/10.1093/cercor/bhq100

Kaidanovich-Beilin, O., T. Lipina, I. Vukobradovic, J. Roder, and J.R. Woodgett. 2011. Assessment of social interaction behaviors. *J. Vis. Exp.* (48):2473. http://dx.doi.org/10.3791/2473

Kalluri, R. 2003. Basement membranes: structure, assembly and role in tumour angiogenesis. *Nat. Rev. Cancer.* 3:422–433. http://dx.doi.org/10.1038/nrc1094

Krook-Magnuson, E., C. Armstrong, M. Oijala, and I. Soltesz. 2013. On-demand optogenetic control of spontaneous seizures in temporal lobe epilepsy. *Nat. Commun.* 4:1376. http://dx.doi.org/10.1038/ncomms2376

Krylova, O., J. Herreros, K.E. Cleverley, E. Ehler, J.P. Henriquez, S.M. Hughes, and P.C. Salinas. 2002. WNT-3, expressed by motoneurons, regulates terminal arborization of neurotrophin-3-responsive spinal sensory neurons. *Neuron.* 35:1043–1056. http://dx.doi.org/10.1016/S0896-6273(02)00860-7

Kucukdereli, H., N.J. Allen, A.T. Lee, A. Feng, M.I. Ozlu, L.M. Conatser, C. Chakraborty, G. Workman, M. Weaver, E.H. Sage, et al. 2011. Control of excitatory CNS synaptogenesis by astrocyte-secreted proteins Hevin and SPARC. *Proc. Natl. Acad. Sci. USA.* 108:E440–E449. http://dx.doi.org/10.1073/pnas.1104977108

Lein, E.S., M.J. Hawrylycz, N. Ao, M. Ayres, A. Bensinger, A. Bernard, A.F. Boe, M.S. Boguski, K.S. Brockway, E.J. Byrnes, et al. 2007. Genome-wide atlas of gene expression in the adult mouse brain. *Nature.* 445:168–176. http://dx.doi.org/10.1038/nature05453

Lewis, D.A., A.A. Curley, J.R. Glausier, and D.W. Volk. 2012. Cortical parvalbumin interneurons and cognitive dysfunction in schizophrenia. *Trends Neurosci.* 35:57–67. http://dx.doi.org/10.1016/j.tins.2011.10.004

Liang, J., W. Xu, Y.T. Hsu, A.X. Yee, L. Chen, and T.C. Südhof. 2015. Conditional neuroligin-2 knockout in adult medial prefrontal cortex links chronic changes in synaptic inhibition to cognitive impairments. *Mol. Psychiatry.* 20:850–859. http://dx.doi.org/10.1038/mp.2015.31

Liao, H.M., Y.L. Chao, A.L. Huang, M.C. Cheng, Y.J. Chen, K.F. Lee, J.S. Fang, C.H. Hsu, and C.H. Chen. 2012. Identification and characterization of three inherited genomic copy number variations associated with familial schizophrenia. *Schizophr. Res.* 139:229–236. http://dx.doi.org/10.1016/j.schres.2012.05.015

Lund, R.D. 1972. Anatomic studies on the superior colliculus. *Invest. Ophthalmol.* 11:434–441.

Maro, G.S., S. Gao, A.M. Olechwier, W.L. Hung, M. Liu, E. Özkan, M. Zhen, and K. Shen. 2015. MADD-4/Punctin and Neurexin organize *C. elegans* GABAergic postsynapses through Neuroligin. *Neuron.* 86:1420–1432. http://dx.doi.org/10.1016/j.neuron.2015.05.015

Martens, H., M.C. Weston, J.L. Boulland, M. Grønborg, J. Grosche, J. Kacza, A. Hoffmann, M. Matteoli, S. Takamori, T. Harkany, et al. 2008. Unique luminal localization of VGAT-C terminus allows for selective labeling of active cortical GABAergic synapses. *J. Neurosci.* 28:13125–13131. http://dx.doi.org/10.1523/JNEUROSCI.3887-08.2008

Matsumoto-Miyai, K., E. Sokolowska, A. Zurlinden, C.E. Gee, D. Lüscher, S. Hettwer, J. Wölfel, A.P. Ladner, J. Ster, U. Gerber, et al. 2009. Coincident pre- and postsynaptic activation induces dendritic filopodia via neurotrypsin-dependent agrin cleavage. *Cell.* 136:1161–1171. http://dx.doi.org/10.1016/j.cell.2009.02.034

Meyer, F., and B. Moussian. 2009. *Drosophila* multiplexin (Dmp) modulates motor axon pathfinding accuracy. *Dev. Growth Differ.* 51:483–498. http://dx.doi.org/10.1111/j.1440-169X.2009.01111.x

Moy, S.S., J.J. Nadler, A. Perez, R.P. Barbaro, J.M. Johns, T.R. Magnuson, J. Piven, and J.N. Crawley. 2004. Sociability and preference for social novelty in five inbred strains: an approach to assess autistic-like behavior in mice. *Genes Brain Behav.* 3:287–302. http://dx.doi.org/10.1111/j.1601-1848.2004.00076.x

Oray, S., A. Majewska, and M. Sur. 2004. Dendritic spine dynamics are regulated by monocular deprivation and extracellular matrix degradation. *Neuron.* 44:1021–1030. http://dx.doi.org/10.1016/j.neuron.2004.12.001

Oudart, J.B., S. Brassart-Pasco, A. Vautrin, C. Sellier, C. Machado, A. Dupont-Deshorgue, B. Brassart, S. Baud, M. Dauchez, J.C. Monboisse, et al. 2015. Plasmin releases the anti-tumor peptide from the NC1 domain of collagen XIX. *Oncotarget.* 6:3656–3668. http://dx.doi.org/10.18632/oncotarget.2849

Oudart, J.B., M. Doue, A. Vautrin, B. Brassart, C. Sellier, A. Dupont-Deshorgue, J.C. Monboisse, F.X. Maquart, S. Brassart-Pasco, and L. Ramont. 2016. The anti-tumor NC1 domain of collagen XIX inhibits the FAK/PI3K/Akt/mTOR signaling pathway through alphavbeta3 integrin interaction. *Oncotarget.* 12:516–528.

Pedersen, C.S., D.B. Sørensen, A.I. Parachikova, and N. Plath. 2014. PCP-induced deficits in murine nest building activity: employment of an ethological rodent behavior to mimic negative-like symptoms of schizophrenia. *Behav. Brain Res.* 273:63–72. http://dx.doi.org/10.1016/j.bbr.2014.07.023

Peixoto, R.T., P.A. Kunz, H. Kwon, A.M. Mabb, B.L. Sabatini, B.D. Philpot, and M.D. Ehlers. 2012. Transsynaptic signaling by activity-dependent cleavage of neuroligin-1. *Neuron.* 76:396–409. http://dx.doi.org/10.1016/j.neuron.2012.07.006

Petitclerc, E., A. Boutaud, A. Prestayko, J. Xu, Y. Sado, Y. Ninomiya, M.P. Sarras Jr., B.G. Hudson, and P.C. Brooks. 2000. New functions for non-collagenous domains of human collagen type IV. Novel integrin

ligands inhibiting angiogenesis and tumor growth in vivo. *J. Biol. Chem.* 275:8051–8061. http://dx.doi.org/10.1074/jbc.275.11.8051

Pfeffer, C.K., M. Xue, M. He, Z.J. Huang, and M. Scanziani. 2013. Inhibition of inhibition in visual cortex: the logic of connections between molecularly distinct interneurons. *Nat. Neurosci.* 16:1068–1076. http://dx.doi.org/10.1038/nn.3446

Pi, H.J., B. Hangya, D. Kvitsiani, J.I. Sanders, Z.J. Huang, and A. Kepecs. 2013. Cortical interneurons that specialize in disinhibitory control. *Nature*. 503:521–524. http://dx.doi.org/10.1038/nature12676

Poulopoulos, A., G. Aramuni, G. Meyer, T. Soykan, M. Hoon, T. Papadopoulos, M. Zhang, I. Paarmann, C. Fuchs, K. Harvey, et al. 2009. Neuroligin 2 drives postsynaptic assembly at perisomatic inhibitory synapses through gephyrin and collybistin. *Neuron.* 63:628–642. http://dx.doi.org/10.1016/j.neuron.2009.08.023

Ramont, L., S. Brassart-Pasco, J. Thevenard, A. Deshorgue, L. Venteo, J.Y. Laronze, M. Pluot, J.C. Monboisse, and F.X. Maquart. 2007. The NC1 domain of type XIX collagen inhibits in vivo melanoma growth. *Mol. Cancer Ther.* 6:506–514. http://dx.doi.org/10.1158/1535-7163.MCT-06-0207

Reif, R., S. Sales, S. Hettwer, B. Dreier, C. Gisler, J. Wölfel, D. Lüscher, A. Zurlinden, A. Stephan, S. Ahmed, et al. 2007. Specific cleavage of agrin by neurotrypsin, a synaptic protease linked to mental retardation. *FASEB J.* 21:3468–3478. http://dx.doi.org/10.1096/fj.07-8800com

Ricard-Blum, S., and L. Ballut. 2011. Matricryptins derived from collagens and proteoglycans. *Front. Biosci. (Landmark Ed.).* 16:674–697. http://dx.doi.org/10.2741/3712

Rossignol, E., I. Kruglikov, A.M. van den Maagdenberg, B. Rudy, and G. Fishell. 2013. CaV 2.1 ablation in cortical interneurons selectively impairs fast-spiking basket cells and causes generalized seizures. *Ann. Neurol.* 74:209–222. http://dx.doi.org/10.1002/ana.23913

Rubenstein, J.L., and M.M. Merzenich. 2003. Model of autism: increased ratio of excitation/inhibition in key neural systems. *Genes Brain Behav.* 2:255–267. http://dx.doi.org/10.1034/j.1601-183X.2003.00037.x

Sachdev, P. 1998. Schizophrenia-like psychosis and epilepsy: the status of the association. *Am. J. Psychiatry.* 155:325–336. http://dx.doi.org/10.1176/ajp.155.3.325

Scheiffele, P. 2003. Cell-cell signaling during synapse formation in the CNS. *Annu. Rev. Neurosci.* 26:485–508. http://dx.doi.org/10.1146/annurev.neuro.26.043002.094940

Scheiffele, P., J. Fan, J. Choih, R. Fetter, and T. Serafini. 2000. Neuroligin expressed in nonneuronal cells triggers presynaptic development in contacting axons. *Cell*. 101:657–669. http://dx.doi.org/10.1016/S0092-8674(00)80877-6

Schwaller, B., I.V. Tetko, P. Tandon, D.C. Silveira, M. Vreugdenhil, T. Henzi, M.C. Potier, M.R. Celio, and A.E. Villa. 2004. Parvalbumin deficiency affects network properties resulting in increased susceptibility to epileptic seizures. *Mol. Cell. Neurosci.* 25:650–663. http://dx.doi.org/10.1016/j.mcn.2003.12.006

Sgadò, P., M. Dunleavy, S. Genovesi, G. Provenzano, and Y. Bozzi. 2011. The role of GABAergic system in neurodevelopmental disorders: a focus on autism and epilepsy. *Int. J. Physiol. Pathophysiol. Pharmacol.* 3:223–235.

Singh, R., J. Su, J. Brooks, A. Terauchi, H. Umemori, and M.A. Fox. 2012. Fibroblast growth factor 22 contributes to the development of retinal nerve terminals in the dorsal lateral geniculate nucleus. *Front. Mol. Neurosci.* 4:61. http://dx.doi.org/10.3389/fnmol.2011.00061

Sommeijer, J.P., and C.N. Levelt. 2012. Synaptotagmin-2 is a reliable marker for parvalbumin positive inhibitory boutons in the mouse visual cortex. *PLoS One.* 7:e35323. http://dx.doi.org/10.1371/journal.pone.0035323

Su, J., K. Gorse, F. Ramirez, and M.A. Fox. 2010. Collagen XIX is expressed by interneurons and contributes to the formation of hippocampal synapses. *J. Comp. Neurol.* 518:229–253. http://dx.doi.org/10.1002/cne.22228

Su, J., C.V. Haner, T.E. Imbery, J.M. Brooks, D.R. Morhardt, K. Gorse, W. Guido, and M.A. Fox. 2011. Reelin is required for class-specific retinogeniculate targeting. *J. Neurosci.* 31:575–586. http://dx.doi.org/10.1523/JNEUROSCI.4227-10.2011

Su, J., R.S. Stenbjorn, K. Gorse, K. Su, K.F. Hauser, S. Ricard-Blum, T. Pihlajaniemi, and M.A. Fox. 2012. Target-derived matricryptins organize cerebellar synapse formation through α3β1 integrins. *Cell Reports.* 2:223–230. http://dx.doi.org/10.1016/j.celrep.2012.07.001

Sumiyoshi, H., K. Inoguchi, M. Khaleduzzaman, Y. Ninomiya, and H. Yoshioka. 1997. Ubiquitous expression of the alpha1(XIX) collagen gene (Col19a1) during mouse embryogenesis becomes restricted to a few tissues in the adult organism. *J. Biol. Chem.* 272:17104–17111. http://dx.doi.org/10.1074/jbc.272.27.17104

Sumiyoshi, H., N. Mor, S.Y. Lee, S. Doty, S. Henderson, S. Tanaka, H. Yoshioka, S. Rattan, and F. Ramirez. 2004. Esophageal muscle physiology and morphogenesis require assembly of a collagen XIX-rich basement membrane zone. *J. Cell Biol.* 166:591–600. http://dx.doi.org/10.1083/jcb.200402054

Suzuki, K., Y. Hayashi, S. Nakahara, H. Kumazaki, J. Prox, K. Horiuchi, M. Zeng, S. Tanimura, Y. Nishiyama, S. Osawa, et al. 2012. Activity-dependent proteolytic cleavage of neuroligin-1. *Neuron.* 76:410–422. http://dx.doi.org/10.1016/j.neuron.2012.10.003

Takahashi, H., K. Katayama, K. Sohya, H. Miyamoto, T. Prasad, Y. Matsumoto, M. Ota, H. Yasuda, T. Tsumoto, J. Aruga, and A.M. Craig. 2012. Selective control of inhibitory synapse development by Slitrk3-PTPδ trans-synaptic interaction. *Nat. Neurosci.* 15:389–398: S1–S2. http://dx.doi.org/10.1038/nn.3040

Terauchi, A., E.M. Johnson-Venkatesh, A.B. Toth, D. Javed, M.A. Sutton, and H. Umemori. 2010. Distinct FGFs promote differentiation of excitatory and inhibitory synapses. *Nature.* 465:783–787. http://dx.doi.org/10.1038/nature09041

Toth, A.B., A. Terauchi, L.Y. Zhang, E.M. Johnson-Venkatesh, D.J. Larsen, M.A. Sutton, and H. Umemori. 2013. Synapse maturation by activity-dependent ectodomain shedding of SIRPα. *Nat. Neurosci.* 16:1417–1425. http://dx.doi.org/10.1038/nn.3516

Tu, H., B. Pinan-Lucarré, T. Ji, M. Jospin, and J.L. Bessereau. 2015. *C. elegans* punctin clusters GABA(A) receptors via neuroligin binding and UNC-40/DCC recruitment. *Neuron.* 86:1407–1419. http://dx.doi.org/10.1016/j.neuron.2015.05.013

Ullian, E.M., K.S. Christopherson, and B.A. Barres. 2004. Role for glia in synaptogenesis. *Glia.* 47:209–216. http://dx.doi.org/10.1002/glia.20082

Umemori, H., M.W. Linhoff, D.M. Ornitz, and J.R. Sanes. 2004. FGF22 and its close relatives are presynaptic organizing molecules in the mammalian brain. *Cell.* 118:257–270. http://dx.doi.org/10.1016/j.cell.2004.06.025

Waites, C.L., A.M. Craig, and C.C. Garner. 2005. Mechanisms of vertebrate synaptogenesis. *Annu. Rev. Neurosci.* 28:251–274. http://dx.doi.org/10.1146/annurev.neuro.27.070203.144336

Wang, T., A.G. Hauswirth, A. Tong, D.K. Dickman, and G.W. Davis. 2014. Endostatin is a trans-synaptic signal for homeostatic synaptic plasticity. *Neuron.* 83:616–629. http://dx.doi.org/10.1016/j.neuron.2014.07.003

Wöhr, M., D. Orduz, P. Gregory, H. Moreno, U. Khan, K.J. Vörckel, D.P. Wolfer, H. Welzl, D. Gall, S.N. Schiffmann, and B. Schwaller. 2015. Lack of parvalbumin in mice leads to behavioral deficits relevant to all human autism core symptoms and related neural morphofunctional abnormalities. *Transl. Psychiatry.* 5:e525. http://dx.doi.org/10.1038/tp.2015.19

Woo, J., S.K. Kwon, J. Nam, S. Choi, H. Takahashi, D. Krueger, J. Park, Y. Lee, J.Y. Bae, D. Lee, et al. 2013. The adhesion protein IgSF9b is coupled to neuroligin 2 via S-SCAM to promote inhibitory synapse development. *J. Cell Biol.* 201:929–944. http://dx.doi.org/10.1083/jcb.201209132

Yin, D.M., Y.J. Chen, A. Sathyamurthy, W.C. Xiong, and L. Mei. 2012. Synaptic dysfunction in schizophrenia. *Adv. Exp. Med. Biol.* 970:493–516. http://dx.doi.org/10.1007/978-3-7091-0932-8_22